Available online at www.sciencedirect.com

ScienceDirect

Advances in Space Research 71 (2023) 4765–4786

ADVANCES IN SPACE RESEARCH (a COSPAR publication)

www.elsevier.com/locate/asr

Implementation and analysis of fault grouping for multi-constellation advanced RAIM

Shizhuang Wang [a], Yawei Zhai [a], Cheng Chi [a], Xingqun Zhan [a,*], Yiping Jiang [b]

[a] School of Aeronautics and Astronautics, Shanghai Jiao Tong University, 200240 Shanghai, China
[b] Department of Aeronautical and Aviation Engineering, The Hong Kong Polytechnic University, 999077, Hong Kong, China

Received 8 April 2022; received in revised form 3 January 2023; accepted 9 January 2023
Available online 31 January 2023

Abstract

The aviation community is pursuing multi-constellation Advanced Receiver Autonomous Integrity Monitoring (ARAIM) to offer safe aircraft navigation services. The computational issue of ARAIM becomes critical when multiple constellations are involved and Fault Exclusion (FE) is enabled. This paper proposes an implementation of fault grouping to improve the efficiency of multi-constellation ARAIM and to benefit navigation performance. To potentially accommodate most ARAIM services, we consider both ARAIM Fault Detection (FD) and ARAIM Fault Detection and Exclusion (FDE) scenarios. In addition, given the difference between Vertical ARAIM (V-ARAIM) and Horizontal ARAIM (H-ARAIM), the implementation steps of fault grouping for V-ARAIM and H-ARAIM are respectively described. More importantly, unlike most of the prior approaches that were limited to dual-constellation scenarios, our implementation can support up to four constellations. The implementation of fault grouping is evaluated using multiple sets of simulations, which are carried out as a function of the number of constellations, prior fault probabilities, error models, and operational services. The results suggest that in most cases, the proposed implementation of fault grouping can effectively reduce the ARAIM computational load while benefiting or maintaining the navigation performance.

Keywords: Advanced Receiver Autonomous Integrity Monitoring (ARAIM); Fault Detection and Exclusion (FDE); Global Navigation Satellite Systems (GNSS); Integrity; Continuity

1. Introduction

To use Global Navigation Satellite Systems (GNSS) for aircraft navigation, potential measurement faults must be considered and their impact on navigation reliability shall be quantified (Pervan 1996; Wang et al. 2018). To this end, integrity is defined to measure the trust that can be placed on the correctness of the navigation solution (ICAO 2009). Ensuring high integrity is the precondition for employing GNSS in safety–critical applications, and thus developing integrity monitoring techniques has always been a crucial topic in aviation navigation (Blanch et al. 2015).

In civil aviation, Receiver Autonomous Integrity Monitoring (RAIM) has been a key function in airborne receivers (Brown 1992). Recently, it has been evolved into Advanced RAIM (ARAIM) with fully refined architectures and user algorithms (Blanch et al. 2015; Joerger et al. 2014; EU-US Cooperation 2016). The basic ARAIM architecture includes the ground segment and the user segment (Blanch et al. 2014). On the ground side, global monitoring stations collect raw GNSS observation data to generate and validate the Integrity Support Message (ISM), which carries information defining Signal-In-Space Ranging

* Corresponding author.
E-mail addresses: sz.wang@sjtu.edu.cn (S. Wang), yawei_zhai@126.com (Y. Zhai), chichengcn@sjtu.edu.cn (C. Chi), xqzhan@sjtu.edu.cn (X. Zhan), yiping.jiang@polyu.edu.hk (Y. Jiang).

https://doi.org/10.1016/j.asr.2023.01.020
0273-1177/

Error (SISRE) and fault statistics (Perea et al. 2017; Walter et al. 2018; Walter et al. 2019; Khanafseh et al. 2015; Zhai et al. 2020; Wang et al. 2021). On the user side, airborne receivers use the measurements and the ISM to perform real-time Fault Detection and Exclusion (FDE) and to evaluate the corresponding Integrity Risk (IR) or Protection Level (PL) (Blanch et al. 2015; Blanch et al. 2017; Blanch et al. 2022; Milner et al. 2017; Joerger and Pervan 2016).

ARAIM is developed to support next-generation Dual-Frequency Multi-Constellation (DFMC) operations. Benefited from DFMC, ARAIM will allow increased service levels globally with minimized investment in the ground infrastructure. Meanwhile, because ARAIM is designed based on Multiple Hypothesis Solution Separation (MHSS), it can monitor multiple faults up to constellation faults to address the issue that the probability of these events occurring cannot be neglected in DFMC operations.

ARAIM can be divided into Horizontal ARAIM (H-ARAIM) and Vertical ARAIM (V-ARAIM) (EU-US Cooperation 2016). H-ARAIM aims at providing horizontal navigation services to support en-route down to non-precision approaches, where Required Navigation Performance (RNP) 0.1 corresponds to the most stringent navigation requirement. V-ARAIM is intended for Localizer Performance with Vertical guidance (LPV) approach procedures, of which the final goal is to lead the aircraft to a 200-foot decision height, i.e., LPV-200. Both H-ARAIM and V-ARAIM require the Fault Detection (FD) function to ensure navigation integrity. As for Fault Exclusion (FE), it is usually not necessary for V-ARAIM, but it must always be implemented for H-ARAIM to satisfy the stringent continuity requirement (Joerger et al. 2020).

Current ARAIM research activities are led by ARAIM Technical Subgroup (TSG) of Working Group C. ARAIM TSG has been focusing on the dual-constellation scenario using Global Positioning System (GPS) and Galileo (EU-US Cooperation 2016). Meanwhile, GLONASS and the third-generation BeiDou System (BDS) will also be available for future use in civil aviation (Yang et al. 2022). However, there have been few investigations on their potential benefits to ARAIM (El-Mowafy and Yang 2016; El-Mowafy 2016). Given that the constellations might be subject to long-term outages or faults (e.g., Galileo in 2019, 7 days; GLONASS in 2014, 11 h) (Inside GNSS 2019; GPS World 2014) and that ARAIM requires at least 2 full constellations, it is imperative to revisit ARAIM with more than two constellations.

Employing more constellations will generally improve ARAIM availability, even though these constellations are subject to higher ISM values (Zhai et al. 2019a). However, Zhai et al. (2019a) also pointed out that involving more constellations will dramatically increase the number of monitored fault hypotheses in the MHSS ARAIM user algorithm, thereby leading to the exponentially increased computational load and making the ARAIM algorithm not executable in real-time. This is particularly true given that (a) exclusion functions must be implemented for H-ARAIM and (b) the prior fault probabilities should be inflated to account for the time correlation effects on IR evaluation (Bang et al. 2019; Zhai et al. 2019b; Milner et al. 2020).

Many techniques to reduce the computational complexity of MHSS have been described. Meng et al. (2019) proposed a fault mode determination method with a feedback scheme. Luo et al. (2020) developed a satellite selection method for ARAIM. Compared to these approaches, fault grouping is widely acknowledged as a more powerful technique (Blanch and Walter 2021). It consolidates the list of fault hypotheses into a set of groups, and each group can be monitored by one single fault-tolerant solution (Walter et al. 2014; Gunning et al. 2019). It is noteworthy that other terms in place of "fault grouping" have been used in the literature, including "fault consolidation" (Blanch et al. 2018, 2022) and "clustered ARAIM" (Orejas and Skalicky 2016). As the precursor of these approaches, the Optimally Weighted Average Solution (OWAS) algorithm was initially proposed by Lee et al. (2005) and was later updated by Lee (2006). The principle of OWAS is directly weighting independent solutions from different constellations. Inspired by this concept, Walter et al. (2014) developed an approach to reduce the number of monitored fault modes for ARAIM FD by grouping the fault modes by constellations.

Recently, there have been various new fault grouping methods or implementations (Ge et al. 2017; Orejas and Skalicky 2016; Orejas et al. 2016; Cassel 2017; Pan et al. 2019; Blanch et al. 2018, 2019, 2022), which usually require an extra search to obtain the monitored fault sets or a method to simplify the computation of subset solutions. Among these approaches, some of them lead to considerable navigation performance degradation, and some others only considered the FD function. In addition, most of them were limited to dual-constellation scenarios. Moreover, these approaches were usually evaluated using too few sets of simulations to prove that they can work well in most operational scenarios.

In response, this paper proposes an implementation of fault grouping to improve the efficiency and performance of multi-constellation ARAIM under various operational scenarios. Our implementation employs the following principles of fault grouping, which were developed in prior studies (Blanch et al. 2018; 2022). First, one can consolidate those hypotheses that contribute the most to computational load but have little effect on IR. Then, the continuity risk allocation should be updated according to the new list of the monitored hypotheses. By doing so, fault grouping has the potential to dramatically reduce the computational load while not degrading the navigation performance significantly (Blanch et al. 2022).

In our implementation, we consider both V-ARAIM FD and H-ARAIM FDE scenarios. Given the difference between V- and H-ARAIM, the implementation steps of fault grouping for them are respectively described. More

importantly, our implementation can support up to four constellations. Therefore, it is expected to accommodate most ARAIM services. The proposed implementation is evaluated with multiple sets of simulations to prove its effectiveness under various scenarios.

The rest of this paper is organized as follows. Section 2 revisits the ARAIM FDE algorithm and identifies the key issues when incorporating more than two constellations. Section 3 describes the general principles of fault grouping, analyzes its impact on navigation performance, and presents the implementation steps for V- and H-ARAIM FD. The proposed implementation is further expanded to include fault exclusion capability in Section 4. Then, Section 5 evaluates the proposed implementation of fault grouping with multiple sets of simulations. Finally, Section 6 draws the conclusion.

2. MHSS-Based ARAIM user Algorithm: A revisit

This section revisits the baseline MHSS ARAIM user algorithm, which incorporates the latest updates on continuity and time correlation effects (Joerger et al. 2020; Milner et al. 2020). Because continuous work is updating the ARAIM user algorithm, it evolves over time. In this paper, we will employ the one that is consistent with most of the literature as the "baseline" version.

2.1. Real-Time FDE process

Fig. 1 summarizes the real-time ARAIM FDE procedures. First, the list of the fault modes that need to be monitored is established. Then, the test thresholds are evaluated and the corresponding IR (or PL) is computed. The remaining tests will be implemented only if the IR requirement (denoted by I_{REQ}) or the Alert Limit (AL) of the intended operation is met. Whether an exclusion should be enabled highly depends on specific operational requirements, and the cases where FE is necessary have been identified in prior studies (Zhai et al. 2018; Joerger et al. 2020).

The normalized detection test statistics q_d is expressed by (Blanch et al. 2015):

$$q_d = \frac{\widehat{x}_0 - \widehat{x}_d}{\sigma_{\Delta_d}} = \frac{\varepsilon_0 - \varepsilon_d}{\sigma_{\Delta_d}} \tag{1}$$

where $\widehat{x}_0$ is the all-in-view position estimate, for a position coordinate of interest; $\widehat{x}_d$ is the position estimate using all the SVs except the one(s) included in subset d, $d = 1, \cdots, h_{bsl}$; the label "bsl" stands for the baseline algorithm; h_{bsl} is the number of monitored fault hypotheses in the FD process; subset d includes all the SV(s) that is assumed to be faulted under fault hypothesis d; σ_{Δ_d} is the standard deviation of the detection statistic Δ_d, $\Delta_d = \widehat{x}_0 - \widehat{x}_d$; ε_0 is the error of $\widehat{x}_0$, having a normal distribution with standard deviation σ_0 and with mean value bounded by b_0; ε_d is the error of $\widehat{x}_d$, following a normal distribution with bounding bias b_d and standard deviation σ_d.

In the detection step, the statistics in (1) are compared with their corresponding thresholds T_d, which are derived in Section 2.2 based on an allocated False Alert (FA) budget. If any test fails, i.e., $\bigcup_{d=1}^{h_{bsl}}(|q_d| > T_d)$, then an alert is issued, indicating that a fault may occur. Otherwise, if all tests pass, i.e., $\bigcap_{d=1}^{h_{bsl}}(|q_d| < T_d)$, then there is no alert, and the operation continues. Hereafter, D_0 denotes the event that there is an alert and $\bar{D}_0$ is its opposite.

If an exclusion function is implemented, it will be executed after an alert occurs. To validate the final exclusion option, second layer detection tests must be employed to confirm that the remaining SVs are Fault Free (FF). The exclusion statistics (i.e., the second layer detection statistics) are defined as (Zhai et al. 2018):

$$q_{e,l} = \frac{\widehat{x}_e - \widehat{x}_{e,l}}{\sigma_{\Delta_{e,l}}} = \frac{\varepsilon_e - \varepsilon_{e,l}}{\sigma_{\Delta_{e,l}}} \tag{2}$$

where $\widehat{x}_e$ is the position estimate using all the SVs except the one(s) included in subset e, $e = 1, \cdots, g_{bsl}$; g_{bsl} is the number of the monitored exclusion candidates in the baseline FE process; $\widehat{x}_{e,l}$ is the position estimate using the remaining SVs after excluding subset e and the second layer subset l, $l = 1, \cdots, s_{bsl}$; s_{bsl} is the number of the second layer fault modes for exclusion candidate e; $\sigma_{\Delta_{e,l}}$ is the standard deviation of the exclusion statistic $\Delta_{e,l}$, $\Delta_{e,l} = \widehat{x}_e - \widehat{x}_{e,l}$; $\varepsilon_{e,l}$ is the error of $\widehat{x}_{e,l}$, having a normal distribution with bounding bias $b_{e,l}$ and standard deviation $\sigma_{e,l}$.

For each exclusion test, the statistics $q_{e,l}$ in (2) are compared to their associated thresholds $T_{e,l}$, which are also derived in Section 2.2 using the allocated continuity budget. If all exclusion tests pass, i.e., $\bigcap_{l=1}^{s_{bsl}}(|q_{e,l}| < T_{e,l})$, the corresponding exclusion candidate (i.e., subset e) is chosen to be excluded. Thus, the event that there is no alert after excluding subset j, labeled as $\bar{D}_j$, is a necessary condition for the event that subset j is excluded (this event is denoted as E_j). It is possible that No Exclusion (NE) is validated, even after testing all the candidates. This case can be expressed as $\bigcap_{e=1}^{g_{bsl}}\{\bigcup_{l=1}^{s_{bsl}}(|q_{e,l}| > T_{e,l})\}$ and will lead to Loss of Continuity (LOC).

2.2. Continuity risk evaluation and FDE thresholds

Continuity measures the capability of a system to perform its function without unscheduled interruptions. Of all the contributions to continuity risk (denoted by P_{LOC}), this paper focuses on the probability of the event that the airborne receiver issues an alert, i.e., P_{alert}. This event can happen under two scenarios: (a) only FD is implemented, and true or false detection occurs; (b) FDE is performed, and detection occurs but the NE option is validated.

For ARAIM FD-only, the FA probability (P_{FA}) is considered as the major contribution to P_{alert}, and it can be expressed and bounded by (Zhai et al. 2018):

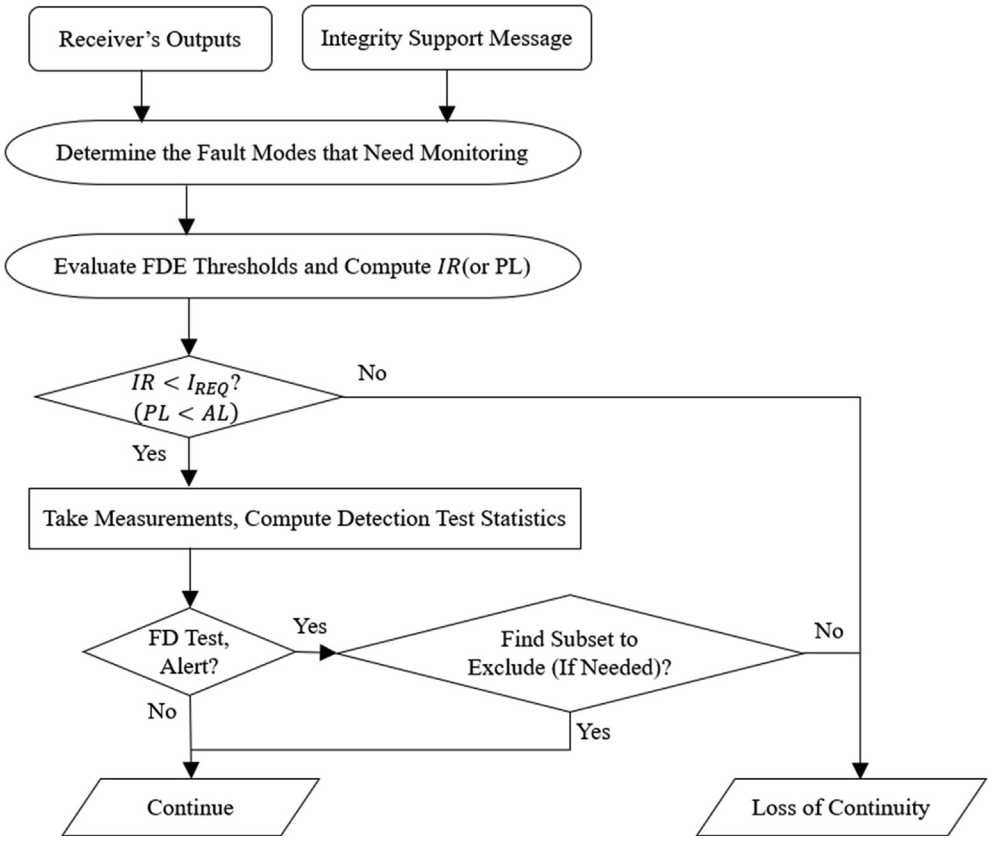

Fig. 1. Flow diagram of the real-time ARAIM FDE implementation.

$$P_{FA} = N_{CONT}^{ES} \cdot P(D_0|H_0)P_{H,0}^{C} < N_{CONT}^{ES} \cdot \sum_{d=1}^{h_{bsl}} P(|q_d| > T_d|H_0)P_{H,0}^{C} \quad (3)$$

where $P_{H,0}^{C}$ is the probability of the FF event for continuity evaluation; N_{CONT}^{ES} is the number of effective samples for continuity evaluation, which captures the impact of test statistic time correlation on P_{LOC} (Zhai et al. 2019b; Milner et al. 2020). As a reminder, H_0 represents the FF event, and D_0 denotes the event that there is an alert when using all the SVs in view, i.e., the first layer detection issues an alert. Let $P_{FA,REQ}$ be the continuity budget allocated to FA events. Then, the FA budget allocated to fault mode d is computed as:

$$P_{FA,d} = \frac{P_{FA,REQ}}{P_{H,0}^{C} \cdot h_{bsl} \cdot N_{CONT}^{ES}} \quad (4)$$

Accordingly, the detection threshold is given by:

$$T_d = Q^{-1}(P_{FA,d}/2) \quad (5)$$

where Q^{-1} is the inverse tail probability function of a zero-mean unit-variance Gaussian distribution.

If FE is implemented, only those detection events that cannot be excluded (i.e., NE) will cause LOC. These events can be further separated into two classes: (a) under FF conditions, a FA followed by NE (FANE), and (b) under faulted conditions, a true FD followed by NE (FDNE). The ARAIM FDE functions must be defined to limit these two events. The probability of FANE and FDNE can be respectively quantified and bounded by (Zhai et al. 2018):

$$P_{FANE} = N_{CONT}^{ES} \cdot P\left(D_0, \bar{E}_0|H_0\right)P_{H,0}^{C} < N_{CONT}^{ES} \cdot \sum_{d=1}^{h_{bsl}} P(|q_d| > T_d|H_0)P_{H,0}^{C} \quad (6)$$

$$P_{FDNE} = N_{CONT}^{ES} \cdot \sum_{j=1}^{g_{bsl}} P\left(D_0, \bar{E}_0|H_j\right)P_{H,j}^{C} < N_{CONT}^{ES} \cdot \sum_{j=1}^{g_{bsl}} \sum_{l=1}^{s_{bsl}} P\left(|q_{j,l}| > T_{j,l}|H_j\right)P_{H,j}^{C} \quad (7)$$

where H_j denotes the j th fault mode (i.e., exclusion candidate) that needs to be considered by the FE function, $j = 1, \cdots, g_{bsl}$. $\bar{E}_0$ represents the NE event. $P_{H,j}^{C}$ is the prior probability of the occurrence of H_j for continuity evaluation, which is derived using the prior probability of SV fault (P_{sat}) and that of constellation fault (P_{const}) with proper conversions to address the exposure time difference (Zhai et al. 2018; Joerger et al. 2020).

By limiting (6) to meet the FANE requirement ($P_{FANE,REQ}$), the continuity budget allocated to fault hypothesis d is obtained:

$$P_{FANE,d} = \frac{P_{FANE,REQ}}{P^{C}_{H,0} \cdot h_{bsl} \cdot N^{ES}_{CONT}}, \quad d = 1, \cdots, h_{bsl} \tag{8}$$

And the corresponding detection threshold is evaluated by:

$$T_d = Q^{-1}(P_{FANE,d}/2) \tag{9}$$

Similarly, by limiting (7) to meet the FDNE requirement ($P_{FDNE,REQ}$), the continuity budget for the l th second layer detection event of the j th exclusion candidate is obtained:

$$P_{FDNE,j,l} = \frac{P_{FDNE,REQ}}{P^{C}_{H,j} \cdot g_{bsl} \cdot s_{bsl} \cdot N^{ES}_{CONT}}, \quad j = 1, \cdots, g_{bsl}, l = 1, \cdots, s_{bsl} \tag{10}$$

And the corresponding threshold is given by:

$$T_{j,l} = Q^{-1}\left(P_{FDNE,j,l}/2\right) \tag{11}$$

2.3. Integrity risk evaluation

As shown in Fig. 1, when evaluating the *a priori* IR, the receiver neither knows whether a fault will be detected or not, nor which SV subset will be excluded. Therefore, all possible integrity threats should be considered.

For ARAIM FD-only, only missed detection events contribute to the final IR. Therefore, the IR of ARAIM FD is a joint probability of having a Hazard Misleading Information (HMI) and sending no alert ($\bar{D}_0$):

$$IR^{bsl}_{FD} = N^{ES}_{INT} \cdot P\left(HMI_0, \bar{D}_0\right) \tag{12}$$

where N^{ES}_{INT} denotes the number of effective numbers for integrity evaluation (Milner et al. 2020). HMI_0 represents the event of HMI existing in the all-in-view solution, i.e., $|\varepsilon_0| > \ell$, where ℓ is the AL. Considering multiple mutually-exclusive fault hypotheses, (12) becomes (Joerger et al. 2014):

$$IR^{bsl}_{FD} = N^{ES}_{INT} \cdot \sum_{i=0}^{h_{sum}} P\left(|\varepsilon_0| > \ell, \bigcap_{d=1}^{h_{bsl}} |q_d| < T_d | H_i\right) P_{H,i} \tag{13}$$

where h_{sum} denotes the total number of all fault hypotheses (including the monitored ones and the others). Then IR^{bsl}_{FD} can be bounded by (Joerger et al. 2014):

$$IR^{bsl}_{FD} < N^{ES}_{INT} \cdot P(|\varepsilon_0| > \ell | H_0) P_{H,0} + N^{ES}_{INT} \cdot \sum_{i=1}^{h_{bsl}} P(|\varepsilon_i| + T_i \sigma_{\Delta_i} > \ell | H_i) P_{H,i} + P^{bsl}_{NM} \tag{14}$$

P^{bsl}_{NM} denotes the sum of the prior probabilities of all the Non-Monitored (NM) fault hypotheses. The determination of the monitored fault modes and the evaluation of P^{bsl}_{NM} will be discussed in Section 2.4.

If FE is implemented, the IR will be computed by:

$$IR^{bsl}_{FDE} = N^{ES}_{INT} \cdot P\left(HMI_0, \bar{D}_0\right) + N^{ES}_{INT} \cdot \sum_{j=1}^{g_{bsl}} P\left(HMI_j, E_j, D_0\right) \tag{15}$$

where HMI_j is the event that HMI exists in a subset solution after excluding the SV(s) in subset j, i.e., $|\varepsilon_j| > \ell$. An upper bound on IR^{bsl}_{FDE} is given as (Zhai et al. 2018):

$$\begin{aligned} \frac{1}{N^{ES}_{INT}}\left(IR^{bsl}_{FDE} - P^{bsl}_{NM}\right) < {} & P(|\varepsilon_0| > \ell | H_0) P_{H,0} \\ & + \sum_{i=1}^{h_{bsl}} P(|\varepsilon_i| + T_i \sigma_{\Delta_i} > \ell | H_i) P_{H,i} \\ & + \sum_{j=1}^{g_{bsl}} \left(P\left(|\varepsilon_j| > \ell | H_0\right) + \sum_{\substack{i=1 \\ s_i \subseteq s_j}}^{h_{bsl}} P\left(|\varepsilon_j| > \ell | H_i\right) P_{H,i} \right. \\ & \left. + \sum_{\substack{i=1 \\ s_i \not\subset s_j}}^{h_{bsl}} P\left(|\varepsilon_{j,i}| + T_{j,i} \sigma_{\Delta_{j,i}} > \ell | H_i\right) P_{H,i} \right) \end{aligned} \tag{16}$$

where S_* is the set of the SVs including in subset *, * = i or j.

2.4. Determination of the list of monitored fault hypotheses

Determining the list of the fault modes that need to be monitored is a key step in the MHSS ARAIM algorithm. The procedures of this step are illustrated as follows and are summarized in Fig. 2.

First, the probability that an SV fault or a constellation fault affects any part of an interval of length T_{EXP} is respectively given by (Blanch et al. 2022):

$$\begin{aligned} \bar{P}_{sat,s} &= \left(1 + \tfrac{T_{EXP}}{MTTN}\right) P_{sat,s}, \ 1 \le s \le n_s \\ \bar{P}_{const,c} &= \left(1 + \tfrac{T_{EXP}}{MTTN}\right) P_{const,c}, \ 1 \le c \le n_c \end{aligned} \tag{17}$$

where $MTTN$ denotes the mean time to notify of the ground segment; the subscript s is the index of the SV, and c is the index of the constellation. n_s denotes the number of visible SVs, and n_c is the number of used constellations. Let $\mathbb{S}_k$ be the set of faulted SVs and $\mathbb{C}_k$ denote the set of faulted constellations under fault hypothesis k. Then the prior probability of fault mode k can be computed by:

$$P_{H,k} = \prod_{s} \bar{P}_{sat,s} \prod_{\substack{s \notin \mathbb{S}_k, \\ \mathbb{C}(s) \notin \mathbb{C}_k}} \left(1 - \bar{P}_{sat,s}\right) \prod_{c \in \mathbb{C}_k} \bar{P}_{const,c} \prod_{c \notin \mathbb{C}_k} \left(1 - \bar{P}_{const,c}\right) \tag{18}$$

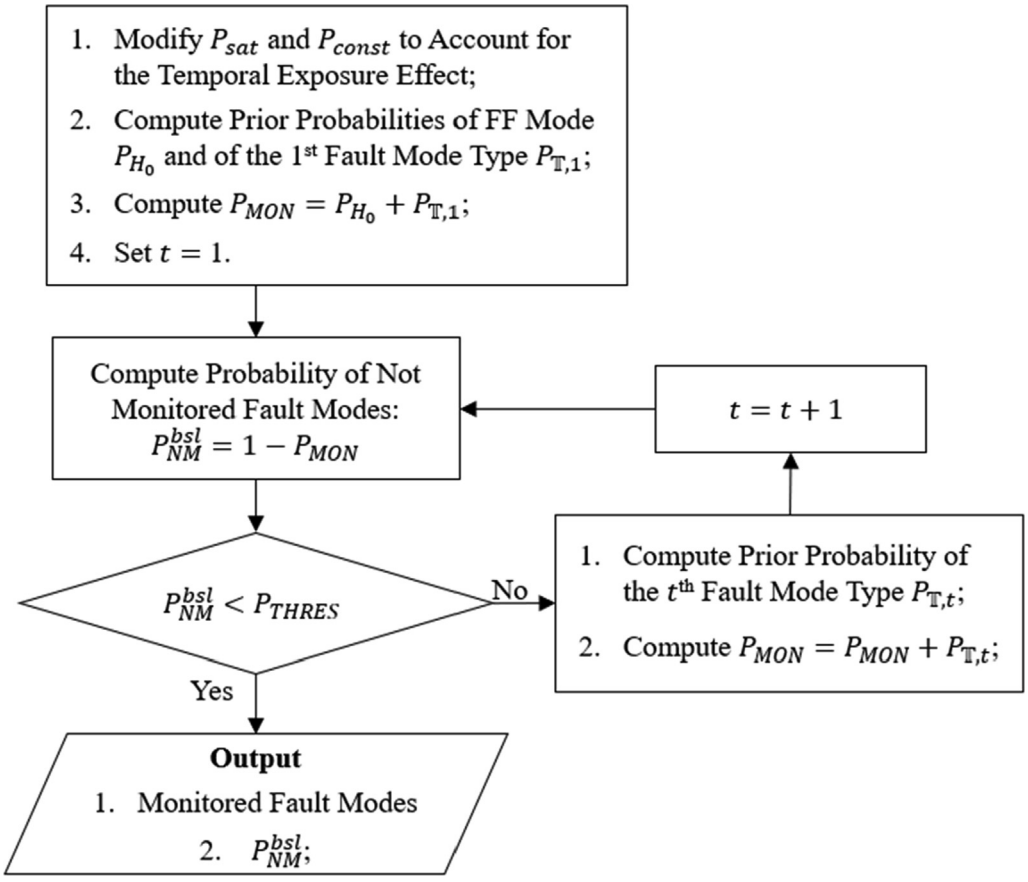

Fig. 2. Flow diagram of the determination of monitored fault modes.

Table 1
Settings of the satellite/constellation fault probabilities and the number of visible SVs, where GAL represents Galileo, and GLO denotes GLONASS.

Constellation	Satellite fault probability		Constellation fault probability		Number of visible SVs
	V-ARAIM	H-ARAIM	V-ARAIM	H-ARAIM	
GPS	10^{-5}	10^{-5}	$[10^{-5}, 10^{-4}]$	10^{-8}	[4,17]
GAL	$[10^{-5}, 10^{-4}]$	$[10^{-5}, 10^{-4}]$	$[10^{-5}, 3 \times 10^{-4}]$	$[10^{-5}, 3 \times 10^{-4}]$	[4,17]
GLO	$[10^{-5}, 10^{-4}]$	$[10^{-5}, 10^{-4}]$	$[10^{-5}, 3 \times 10^{-4}]$	$[10^{-5}, 3 \times 10^{-4}]$	[4,17]
BDS	$[10^{-5}, 10^{-4}]$	$[10^{-5}, 10^{-4}]$	$[10^{-5}, 3 \times 10^{-4}]$	$[10^{-5}, 3 \times 10^{-4}]$	[4,17]

where $\mathbb{c}(s)$ is a function that returns the constellation index of satellite s. The first term corresponds to the faulted SVs, the second term comes from the healthy SVs that belong to the healthy constellations, and the last two terms are respectively associated with the faulted and healthy constellations.

It can be verified that under the settings shown in Table 1, there are at most 8 types of fault modes worth monitoring, even if four constellations are employed. Other fault modes are left unmonitored due to low probability of occurrence, and their prior probabilities are accounted in P_{NM}^{bsl}. Note that the values in Table 1 are selected to reflect the constellation performance commitments (Blanch et al. 2021) and to have a certain robustness. These 8 fault Mode Types (MTs), labelled by $\mathbb{T}_t$, are summarized in Table 2. The last column gives the number of fault modes in each MT, where C_n^k is the number of k-combinations of n elements, and $n_{s,c}$ is the number of visible SVs in constellation c.

There is no need to always monitor all of these 8 MTs, and a possible approach to determine the list of monitored MTs is presented below. It is sufficient to only monitor the first m_{bsl} MTs if we have:

$$P_{NM}^{bsl} = 1 - P_{H,0} - \sum_{t=1}^{m_{bsl}} P_{\mathbb{T},t} < P_{THRES} \tag{19}$$

where $P_{\mathbb{T},t}$ denotes the sum of the probabilities for all the fault modes included in $\mathbb{T}_t$, and P_{THRES} is the threshold for the IR from unmonitored fault modes. Since (18) gives the probabilities of each fault mode, the evaluation of $P_{\mathbb{T},t}$ is straightforward and not stated here for brevity.

Table 2
Illustration of 8 types of fault modes.

Type	Description	Number
$\mathbb{T}_1$	Single constellation fault	$n_1 = n_c$
$\mathbb{T}_2$	Single SV fault	$n_2 = n_s$
$\mathbb{T}_3$	Dual SV faults from one constellation	$n_3 = \sum_{c=1}^{n_c} C_{n_{s,c}}^2$
$\mathbb{T}_4$	Dual SV faults from two constellations	$n_4 = C_{n_s}^2 - n_3$
$\mathbb{T}_5$	Single constellation fault plus a single SV fault from another constellation	$n_5 = (n_c - 1)n_s$
$\mathbb{T}_6$	Dual constellation faults	$n_6 = C_{n_c}^2$
$\mathbb{T}_7$	Three or more SV faults from one constellation	Many
$\mathbb{T}_8$	Other fault modes within two constellations	Many

Please note that if $\mathbb{T}_7$ and/or $\mathbb{T}_8$ are monitored, the fault hypotheses in them will be respectively grouped into $\mathbb{T}_1$ and $\mathbb{T}_6$ by default. The principles and benefits of this grouping operation are illustrated with an example as follows. If "three or more GPS SV faults" hypotheses (in $\mathbb{T}_7$) are monitored, they will be grouped into the GPS constellation fault (in $\mathbb{T}_1$). The grouping operation includes two steps. First, those "three or more GPS SV faults" hypotheses are no longer monitored, which will greatly reduce the computational load. Second, the prior probabilities of these hypotheses are added to the prior probability of the GPS constellation fault. This operation is safe from the integrity perspective, because the subset solution of the GPS constellation fault mode is tolerant to all the faults within this constellation (Walter et al. 2014). In addition, under the settings in Table 1, this step will lead to negligibly small increase in the probability of the GPS constellation fault, thereby not degrading the integrity performance.

The number of monitored hypotheses (h_{bsl}) directly influences the computational cost (Walter et al. 2014; Ge et al. 2017). As an example, Fig. 3 presents h_{bsl} as a function of visible SVs for GPS-Galileo V-ARAIM and H-ARAIM FD. In this figure, we assume that the number of visible SVs from each constellation varies from 5 to 11 and use nominal P_{sat}/P_{const} values of $10^{-5}/10^{-4}$. The result

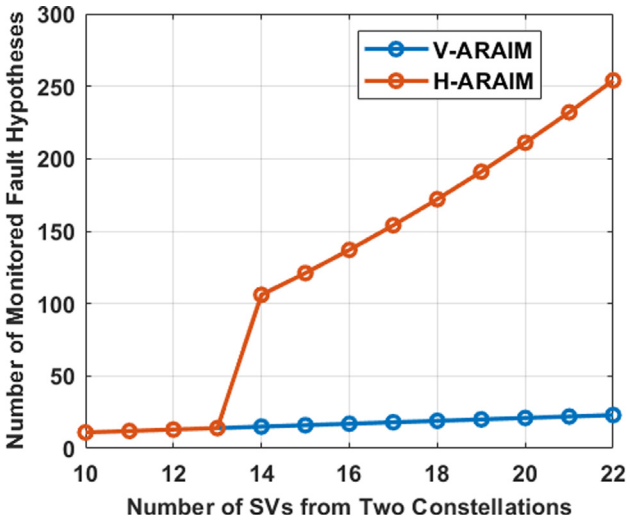

Fig. 3. Numbers of monitored fault hypotheses of GPS-Galileo V-ARAIM and H-ARAIM FD.

suggests a noticeable difference in h_{bsl} between V-ARAIM and H-ARAIM, for which the reason is explained as follows. For V-ARAIM, T_{EXP} is far smaller than $MTTN$, and thus the modification in (17) will cause little impact. With $\bar{P}_{sat}/\bar{P}_{const}$ being $10^{-5}/10^{-4}$ and P_{THRES} being 8×10^{-8}, only monitoring $\mathbb{T}_1$ and $\mathbb{T}_2$ can always ensure P_{NM}^{bsl} smaller than P_{THRES}. In contrast, for H-ARAIM operations, the inflations on P_{sat} and P_{const} lead to significantly larger $\bar{P}_{sat}/\bar{P}_{const}$ values, thereby dramatically increasing h_{bsl}. Specifically, the first four MTs ($\mathbb{T}_1 \sim \mathbb{T}_4$) need to be monitored in this case.

In addition, enabling FE will cause more serious computational issues, because implementing FE requires monitoring all the second layer fault modes for all exclusion candidates. According to (16), the total number of monitored hypotheses for ARAIM FDE can approximate to $g_{bsl} \times h_{bsl}$.

Table 3 shows the numbers of subsets for both V-ARAIM FD and H-ARAIM FDE with different constellation configurations. To capture the sensitivities over satellite fault probability, two sets of P_{sat} values are considered for non-GPS constellations, and they are distinguished using an indicator in Table 3: N represents a nominal P_{sat} of 10^{-5}, and D corresponds to a degraded P_{sat} of 10^{-4}. For these constellations, P_{const} is always set to 10^{-4}. For GPS, a nominal P_{sat} of 10^{-5} is always used, and its P_{const} is set to 10^{-4} for V-ARAIM and 10^{-8} for H-ARAIM, respectively (Walter et al. 2019). Note that this table only shows a rough assessment at one epoch. Besides, the numbers in the last column may vary with different FE algorithms. Nevertheless, this table visualizes how heavy the computational load can be, and it is this kind of evaluation that led to the development of fault grouping. Therefore, we propose an implementation of fault grouping to reduce the computational load of multi-constellation ARAIM.

3. An implementation of fault grouping for ARAIM FD

In this section, we provide a detailed implementation of fault grouping for ARAIM FD. First, we describe the principle of fault grouping in detail, based the investigations in prior studies (Blanch et al. 2018, 2022). Then, the impact of fault grouping on navigation performance is analyzed. Finally, given the difference between V- and H-ARAIM,

Table 3
Numbers of monitored subsets of the baseline MHSS ARAIM user algorithm.

Constellations	V-ARAIM, FD Only		H-ARAIM, FDE	
	Monitored MTs	Subset No.:h_{bsl}	Monitored MTs	Subset No.:$g_{bsl} \times h_{bsl}$
GPS + GAL(N)	1, 2	20	1, 2, 3, 4	3260
GPS + GAL(D)	1, 2, 3, 4, 5	190	1, 2, 3, 4	3260
GPS + GAL(N) + BDS(N)	1, 2, 3, 4, 5	440	1, 2, 3, 4, 5	12,040
GPS + GAL(D) + BDS(D)	1, 2, 3, 4, 5	440	1, 2, 3, 4, 5	157,700
GPS + GAL(N) + BDS(N) + GLO(N)	1, 2, 3, 4, 5	700	1, 2, 3, 4, 5, 6	25,050
GPS + GAL(N) + BDS(D) + GLO(D)	1, 2, 3, 4, 5	700	1, 2, 3, 4, 5, 6	404,850

the key steps to implement the fault grouping scheme to V-ARAIM and H-ARAIM are respectively established.

3.1. Motivation and principles of fault grouping

In Section 2.4, Fig. 3 and Table 3 imply that the number of monitored hypotheses jumps when "dual SV faults" events (i.e., $\mathbb{T}_3$ and $\mathbb{T}_4$) are monitored. This is due to the mathematical feature of combination: the number of visible SVs (n_s) in a multi-constellation scenario is usually about 20 or more, and then the number of 2-combinations from a set of n_s elements can easily go up to hundreds.

To have a clearer view, Fig. 4 presents an analysis of the weight of these fault modes over all the monitored events for ARAIM FD. For Fig. 4a, a nominal P_{sat} of 10^{-5} is applied for all constellations; for Fig. 4b, a degraded P_{sat} of 10^{-4} is applied for the constellations marked in red. For each configuration, column 1 shows the percentage of the number of "dual SV faults" modes over h_{bsl}, and column 2 is the ratio of the sum of the probabilities for these fault modes (i.e., $P_{\mathbb{T},3} + P_{\mathbb{T},4}$) over the that of all the monitored events except FF (i.e., $1 - P_{H,0} - P_{NM}^{bsl}$). This figure suggests that "dual SV faults" hypotheses cause most of the computational burden while having a small weight in IR evaluation.

Therefore, monitoring as few "dual SV faults" modes as possible is an effective approach to reduce the computational cost. However, simply leaving these fault modes unmonitored will sharply increase P_{NM} and even make it exceed the preset threshold, P_{THRES}. As shown in prior studies (Blanch et al. 2018, 2022), a useful idea is to group "dual SV faults" into constellation faults. In the following, we revisit the basic principles of this idea while taking multi-constellation scenarios into account.

For the "dual SV faults from one constellation" modes in $\mathbb{T}_3$, it can be grouped into the corresponding constellation fault in $\mathbb{T}_1$ (Blanch et al. 2018). As an illustrative example, Fig. 5 shows how "dual GPS SV faults" hypotheses are grouped into the GPS constellation fault. As shown in this figure, "dual GPS SV faults" hypotheses will no longer be monitored after the grouping step is executed, thereby reducing the number of subsets.

After fault grouping, the prior probability of the constellation fault hypothesis should be updated (Blanch et al. 2022). Let k_c denote the fault mode corresponding to the fault of constellation c only, and $\mathbb{M}_c$ the set of the fault modes that are grouped into constellation c, except k_c itself. Then, the probability of the new constellation fault mode, which is indexed by k_c' after grouping, is computed as:

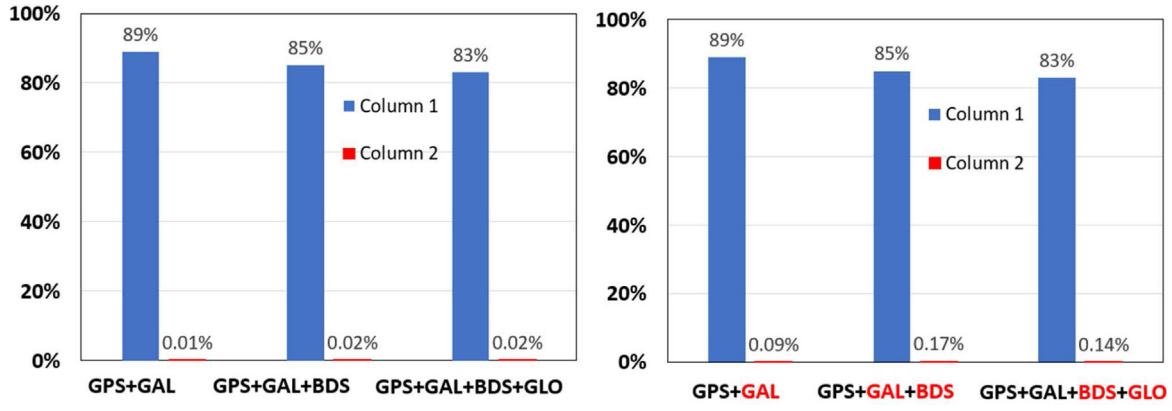

(a) Nominal P_{sat} (b) Degraded P_{sat}

Fig. 4. Percentages of "dual SV faults" modes over all the monitored fault modes in terms of the number of subsets (column 1) and the sum of probabilities (column 2).

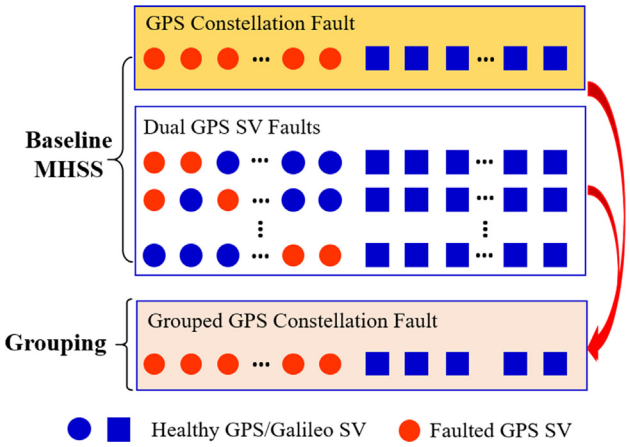

Fig. 5. Illustration of fault grouping using GPS fault modes as an example, where the red arrows indicate that all the fault modes are grouped into a new GPS constellation fault hypothesis.

$$P^{grp}_{H,k'_c} = P_{H,k_c} + \sum_{k\in\mathbb{M}_c} P_{H,k} \tag{20}$$

where the label "*grp*" indicates that this variable is evaluated after grouping. At the same time, the false alert budget for the constellation fault should be updated in a similar way:

$$P^{grp}_{FA,k'_c} = P_{FA,k_c} + \sum_{k\in\mathbb{M}_c} P_{FA,k} \tag{21}$$

where $P_{FA,k}$ denotes the FA budget for fault mode k before grouping, which is evaluated using (4).

Together with Fig. 5, (20) and (21) describe the general principles of fault grouping, which are summarized as follows. For simplicity, we employ the following notations: a set of hypotheses in $\mathbb{M}_k$ (e.g., dual GPS SV faults) are grouped into the hypothesis k (e.g., the GPS constellation fault) to form a new hypothesis; the new hypothesis is indexed by k' in the new list of monitored hypotheses after fault grouping. During the grouping process, one should do the following:

(a) Removing the fault hypotheses in $\mathbb{M}_k$;
(b) Calculating the prior probability of the new hypothesis k' by adding the probabilities for all the hypotheses in $\mathbb{M}_k$ to the probability of the hypothesis k, as shown in (20).
(c) Computing the FA budget of the new hypothesis k' by adding the budgets for all the hypotheses in $\mathbb{M}_k$ to the budget for the hypothesis k, as shown in (21).

Finally, Table 4 shows various fault grouping options that can be applied to multi-constellation ARAIM FD. All of these options can effectively reduce the computational load. However, some of them may not be implemented under specific scenarios because they may obviously degrade navigation performance. Therefore, we will next analyze the impact of fault grouping on navigation performance.

3.2. Impact of fault grouping on navigation performance

Fault grouping can reduce computational load, and meanwhile it will influence navigation performance. After fault grouping, the monitored fault hypotheses can be divided into two categories: C1 denotes the set of the hypotheses that are not involved in the grouping process, and C2 includes the newly formed hypotheses (e.g., the grouped constellation fault in Fig. 5). Fig. 6 further illustrates the fault grouping process by comparing the hypotheses before and after grouping. In this figure, each T-shaped polygon represents a *Grouping Unit* (GU), which depicts how multiple hypotheses are grouped to form a new hypothesis. It is noteworthy that the grouping units are independent of each other.

After fault grouping, the integrity risk of ARAIM FD becomes:

$$\begin{aligned}\frac{IR^{grp}_{FD} - P^{grp}_{NM}}{N^{ES}_{INT}} < {} & P(|\varepsilon_0| > \ell|H_0)P_{H,0} \\ & + \sum_{k\in C1} P(|\varepsilon_k| + T_k\sigma_{\Delta_k} > \ell|H_k)P_{H,k} \\ & + \sum_{k\in C2} P(|\varepsilon_k| + T^{grp}_k\sigma_{\Delta_k} > \ell|H_k)P^{grp}_{H,k}\end{aligned} \tag{22}$$

where T_k is evaluated using (4) and (5), and T^{grp}_k is computed by:

$$T^{grp}_k = Q^{-1}\left(P^{grp}_{FA,k}/2\right), \quad k \in C2 \tag{23}$$

In the right-hand side of (22), the first term denotes the IR from the FF event, the second term is the total IR contribution from C1, and the third term represents the IR coming from the fault hypotheses in C2. Because the fault

Table 4
Various fault grouping options for multi-constellation ARAIM FD.

Hypotheses in $\mathbb{M}_k$	Hypothesis k	Symbol
Single SV fault	Single const. fault	$\mathbb{T}_2 \rightarrow \mathbb{T}_1$
Dual SV faults from one const.	Single const. fault	$\mathbb{T}_3 \rightarrow \mathbb{T}_1$
Single SV fault Dual SV faults from one const.	Single const. fault	$\mathbb{T}_2+\mathbb{T}_3 \rightarrow \mathbb{T}_1$
Dual SV faults from two const.	Single const. fault & one SV fault from another const.	$\mathbb{T}_4 \rightarrow \mathbb{T}_5$
Dual SV faults from two const Single const. fault & one SV fault from another const.	Dual const. faults	$\mathbb{T}_4+\mathbb{T}_5 \rightarrow \mathbb{T}_6$

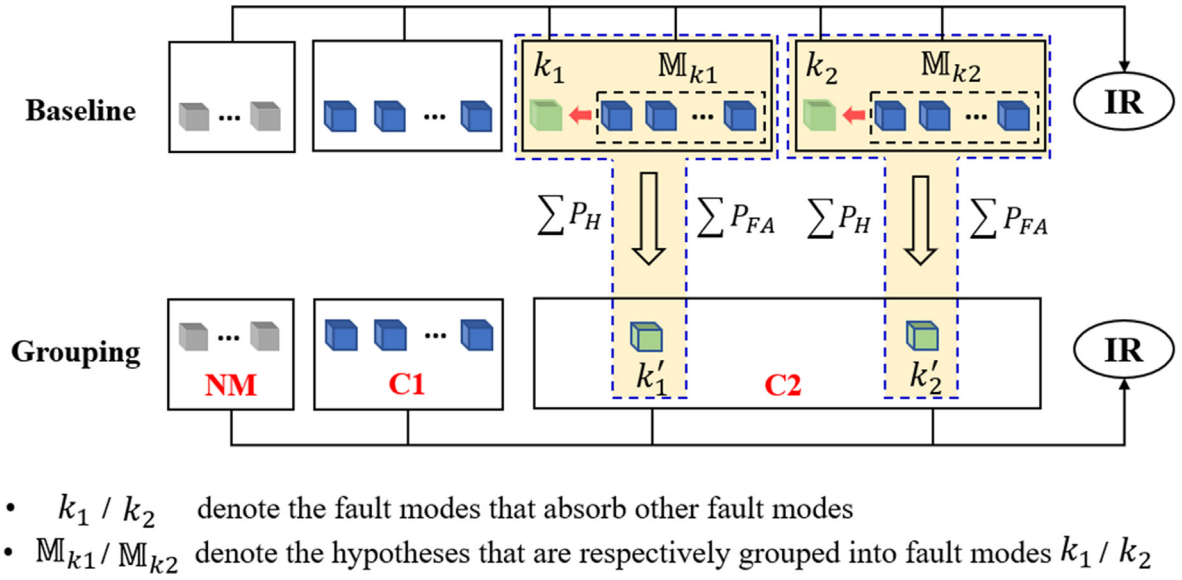

Fig. 6. Graphical illustration of the fault grouping process, where each cube denotes a fault hypothesis, and "NM" stands for "not monitored".

modes in C1 are not involved in the grouping process, their prior probabilities and FA budgets are the same as those in the baseline algorithm. Therefore, the IR from C1 does not change before and after fault grouping.

It is therefore the hypotheses in C2 that determine whether the navigation performance is improved or degraded by fault grouping. The fault grouping process may involve one or multiple grouping units, as shown in Fig. 6. Let us start from one grouping unit to analyze its impact. Assuming that a set of hypotheses in $\mathbb{M}_k$ are grouped into fault hypothesis k to form the new hypothesis k' in C2. For hypothesis k' in C2, its contribution to the IR is expressed as:

$$IR_{k'}^{grp} < N_{INT}^{ES} \cdot P\left(|\varepsilon_k| + T_{k'}^{grp}\sigma_{\Delta_k} > \ell | H_k\right) \cdot P_{H,k'}^{grp} \tag{24}$$

In the baseline MHSS, the IR contributions from hypothesis k and $\mathbb{M}_k$ can be respectively computed by:

$$IR_k^{bsl} < N_{INT}^{ES} \cdot P(|\varepsilon_k| + T_k\sigma_{\Delta_k} > \ell | H_k) P_{H,k} \tag{25}$$

$$IR_{\mathbb{M}_k}^{bsl} < N_{INT}^{ES} \cdot \sum_{i \in \mathbb{M}_k} P(|\varepsilon_i| + T_i\sigma_{\Delta_i} > \ell | H_i) P_{H,i} \tag{26}$$

By comparing $IR_{k'}^{grp}$ with $IR_k^{bsl}+IR_{\mathbb{M}_k}^{bsl}$, one can determine whether this grouping unit degrades the navigation performance. Specifically, the grouping unit benefits the navigation performance if $IR_{k'}^{grp}$ is smaller than$IR_k^{bsl} + IR_{\mathbb{M}_k}^{bsl}$. On the contrary, if $IR_{k'}^{grp}$ is much larger than $IR_k^{bsl}+IR_{\mathbb{M}_k}^{bsl}$, it means that the navigation performance is seriously degraded by fault grouping. In the latter case, the grouping unit should not be implemented so as to maintain navigation availability.

Most of the existing fault grouping approaches reduce the computational load at a cost of noticeable navigation performance degradation. However, fault grouping can actually improve the navigation performance if it is properly implemented (Blanch et al. 2022). This can be proved by analyzing (24) ~ (26) in depth as follows.

Usually, the IR contribution from $\mathbb{M}_k$ is considerably smaller than that from fault mode k. This is because (a) the fault modes in $\mathbb{M}_k$ usually have much lower prior probability than fault mode k, and (b) their conditional IRs, i.e., $P(|\varepsilon_i| + T_i\sigma_{\Delta_i} > \ell | H_i)$, are also significantly smaller than that of fault mode k. Therefore, we can simply compare $IR_{k'}^{grp}$ with IR_k^{bsl} to check whether the fault grouping unit benefits the navigation performance.

By substituting (20) and (21) into (24) and (25), we can find that after fault grouping, the prior probability of fault mode k is increased, i.e., $P_{H,k'}^{grp} > P_{H,k}$, whereas the detection threshold is reduced, i.e., $T_{k'}^{grp} < T_k$, resulting from the increased FA budget. If the first effect drives the IR, then the performance will be degraded; otherwise, the performance will be improved. For demonstration purposes, an example is presented below, where all "dual BDS SV faults" events are grouped into the BDS constellation fault.

The example geometry is established for a user position in Shanghai (Lat: 31.23°; Lon: 121.47°). The required parameters to compute IR are obtained under the V-ARAIM nominal simulation condition defined in Section 5, using a GPS/Galileo/BDS triple-constellation configuration. With the baseline MHSS, the first five MTs (i.e., $\mathbb{T}_1 \sim \mathbb{T}_5$) will be monitored. Now we employ BDS as an example to show the grouping effect.

At the example snapshot, the number of BDS SVs is 14. Before grouping, 91 "dual SV faults from BDS" hypotheses and 1 BDS constellation fault mode are independently monitored. The prior probability of each "dual BDS SV faults" hypothesis is 10^{-10}, and this value is 10^{-4} for the BDS constellation fault. Besides, the FA budget allocated to each of these fault modes is equal to 7.5×10^{-9}. Therefore, the test threshold for the BDS constellation fault is

Table 5
Comparison of the IR contributions from the BDS constellation fault at the example snapshot.

Vertical AL (VAL)	Baseline (IR_k^{bsl}) $T_k = 5.78$	Grouping ($IR_{k'}^{grp}$) $T_{k'}^{grp} = 4.56$
10 *m*	6.09×10^{-9}	8.42×10^{-16}
15 *m*	4.36×10^{-21}	8.05×10^{-29}
20 *m*	8.23×10^{-42}	1.97×10^{-50}
35 *m*	5.22×10^{-156}	2.60×10^{-167}

5.78. After grouping "dual BDS SV faults" into the BDS constellation fault, the grouped BDS constellation fault hypothesis has a prior probability of $10^{-4} + 9.1 \times 10^{-9}$ and a FA budget of 6.9×10^{-7}. Consequently, for the BDS constellation fault mode, the test threshold is reduced from 5.78 to 4.56, whereas the increment on the prior probability is negligibly small. Table 5 compares the IR contributions from the BDS constellation fault mode before and after fault grouping, and the result suggests that grouping "dual BDS SV faults" into the BDS constellation fault can reduce the computational load while benefiting the navigation performance.

Unlike the example above, there are some scenarios where grouping the hypotheses in $\mathbb{M}_k$ into fault mode k makes the probability of the new hypothesis k' much higher than that of fault mode k. In these situations, the navigation performance may still be improved or only slightly degraded. For further illustration, we present an example of such situations, where "1 GPS SV fault plus 1 BDS SV fault", "GPS constellation fault plus 1 BDS SV fault", and "BDS constellation fault plus 1 GPS SV fault" hypotheses are all grouped into the "GPS-BDS dual constellation faults" hypothesis.

This example scenario is almost the same as the previous one, except that four constellations are employed here. The numbers of visible SVs are 7/9/8/14 for GPS/Galileo/GLONASS/BDS. Before grouping, the "GPS-BDS dual constellation faults" hypothesis has a prior probability of 10^{-8} and is allocated with a FA budget of 3.5×10^{-9}. After fault grouping, the prior probability of the grouped "GPS-BDS dual constellation faults" hypothesis becomes 4.1×10^{-8}, and its FA budget is increased to 4.2×10^{-7}. Obviously, the prior probability of this hypothesis becomes four times the original one. Table 6 compares the IR contributions from this fault mode before and after grouping. The result indicates that the navigation performance can be benefited by fault grouping even though the increment on the prior probability is considerably large.

Table 6
Comparison of the IR contributions from the "GPS-BDS dual constellation faults" hypothesis before and after fault grouping.

Vertical AL (VAL)	Baseline (IR_k^{bsl}) $T_k = 5.91$	Grouping ($IR_{k'}^{grp}$) $T_{k'}^{grp} = 5.05$
10 *m*	8.74×10^{-14}	4.09×10^{-14}
15 *m*	1.85×10^{-28}	9.76×10^{-30}
20 *m*	1.93×10^{-53}	1.10×10^{-55}
35 *m*	9.37×10^{-191}	6.61×10^{-196}

Table 7
Comparison of the IR contributions from the "GPS-BDS dual constellation faults" before and after fault grouping, where P_{sat} is 10^{-4} for all constellations.

Vertical AL (VAL)	Baseline (IR_k^{bsl}) $T_k = 5.91$	Grouping ($IR_{k'}^{grp}$) $T_{k'}^{grp} = 5.05$
10 *m*	8.74×10^{-14}	1.21×10^{-12}
15 *m*	1.85×10^{-28}	2.86×10^{-28}
20 *m*	1.93×10^{-53}	3.25×10^{-54}
35 *m*	1.12×10^{-191}	1.94×10^{-194}

Finally, a more extreme example scenario is established by setting P_{sat} to 10^{-4} for all constellations while leaving other parameters unchanged. In this scenario, the prior probability of the "GPS-BDS dual constellation faults" hypothesis is increased by a factor of 120, from 10^{-8} to 1.2×10^{-6}, after fault grouping. The new IR result is given in Table 7, and we can find that (a) for VAL being 35 or 20 m, the navigation performance is still improved, whereas (b) the performance is degraded when VAL is 15 or 10 m. This result suggests that one can still try to group "dual SV faults from two constellations" and "single constellation fault plus one SV fault" into "dual constellation faults" even if this may increase the prior probability of the "dual constellation faults" hypothesis by a large factor. This lays a key foundation for the fault grouping scheme applied to multi-constellation ARAIM.

To conclude, fault grouping can effectively reduce the computational load while possibly benefiting the navigation performance. This is because from the perspective of IR, the positive effect resulting from the decrease in the detection threshold may compensate the negative effect caused by the increase in the prior probability. In addition to the cases where a grouping unit results in small increase in the prior probability but significant decrease in the detection threshold, the navigation performance might also be benefited by fault grouping in the scenarios where the prior probability is dramatically increased. Therefore, to determine whether a grouping unit should be implemented, a possible approach would be to directly compare the IR contributions before and after grouping, as shown in Tables 5–7.

3.3. Implementation of the fault grouping scheme to Multi-Constellation V-ARAIM

Incorporating the existing fault grouping approaches and involving new grouping strategies, this subsection provides a detailed, robust, and flexible implementation of fault grouping for V-ARAIM. Unlike most approaches that are designed for dual-constellation ARAIM, our implementation can support up to four constellations, thereby enabling a wider range of operational scenarios.

In the baseline MHSS, the list of monitored MTs varies with (a) the number of constellations in use, (b) the number

Table 8
Four lists of monitored fault hypotheses for multi-constellation V-ARAIM before grouping.

Symbol	Description	Number of Subsets
$\mathbb{L}_1^{\mathrm{V}}$	Single const. fault ($\mathbb{T}_1$); single SV fault ($\mathbb{T}_2$)	$n_{\mathbb{L}1} = n_s + n_c$
$\mathbb{L}_2^{\mathrm{V}}$	$\mathbb{L}_1^{\mathrm{V}}$; dual SV faults from one const. ($\mathbb{T}_3$)	$n_{\mathbb{L}2} = n_{\mathbb{L}1} + \sum_{c=1}^{n_c} C_{n_{s,c}}^2$
$\mathbb{L}_3^{\mathrm{V}}$	$\mathbb{L}_2^{\mathrm{V}}$; one const. fault plus one SV fault ($\mathbb{T}_5$)	$n_{\mathbb{L}3} = n_{\mathbb{L}2} + (n_c - 1)n_s$
$\mathbb{L}_4^{\mathrm{V}}$	$\mathbb{L}_3^{\mathrm{V}}$; dual SV faults from two const. ($\mathbb{T}_4$); dual const. faults ($\mathbb{T}_6$)	$n_{\mathbb{L}4} = n_c(n_s + 1) + C_{n_s}^2 + C_{n_c}^2$

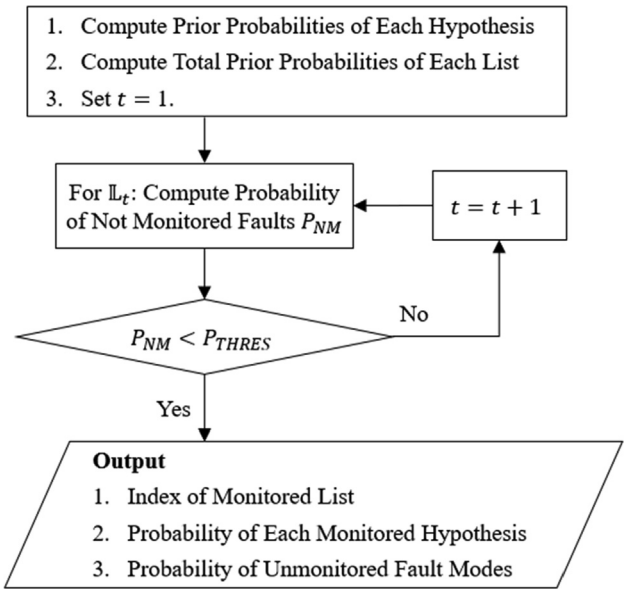

Fig. 7. Flowchart of the determination of the monitored list.

of visible SVs, and (c) the settings on the satellite and constellation fault probabilities. For the convenience of implementing fault grouping, we provide four fixed lists of monitored MTs in Table 8. The user should choose ONE of these lists through a search process, as shown in Fig. 7. Please note that in $\mathbb{L}_4$, "three or more SV faults from one constellation" ($\mathbb{T}_7$) and "other fault modes within two constellations" ($\mathbb{T}_8$) hypotheses have already been respectively grouped into $\mathbb{T}_1$ and $\mathbb{T}_6$. This can reduce the IR from unmonitored faults while avoiding increasing the number of subsets.

After determining which list to be monitored, the FA budget should be allocated to each monitored hypothesis using (4). The next step is applying fault grouping to the monitored hypotheses. In the following, we will discuss how to implement fault grouping to each list.

(1) Fault grouping for List 1 ($\mathbb{L}_1^{\mathrm{V}}$):

This list is mainly for the dual-constellation scenarios with low satellite fault probability. For each constellation, we can group the "single SV fault" hypotheses to the constellation fault. Prior studies have proved that with two constellations, grouping single SV faults by constellation can improve the navigation performance (Zhai et al. 2019a; Walter et al. 2014).

(2) Fault grouping for List 2 ($\mathbb{L}_2^{\mathrm{V}}$):

For this list, an effective approach would be to group "dual SV faults from one constellation" hypotheses by constellation. This operation tends to always benefit the navigation performance, because it leads to small increase in the prior probability of the constellation fault while significantly reducing the detection threshold (see Table 5). It is noteworthy that "grouping single SV fault by constellation" is not implemented here. This is because P_{sat} is close to or even higher than P_{const} in this case, and this grouping option will seriously increase the prior probability of the constellation fault.

(3) Fault grouping for List 3 ($\mathbb{L}_3^{\mathrm{V}}$):

For this list, we apply the same grouping operation as $\mathbb{L}_2^{\mathrm{V}}$ to the monitored fault modes. In addition to the hypotheses in $\mathbb{L}_2$, this list also includes the "single constellation fault plus one SV fault from another constellation" hypotheses. However, these newly monitored fault modes cannot be grouped into other monitored hypotheses, and thus they are not involved in the grouping process.

(4) Fault grouping for List 4 ($\mathbb{L}_4^{\mathrm{V}}$):

In the lists above, two SV faults from different constellations are left unmonitored, because the number of this type of fault modes is very large while the sum of their prior probabilities is relatively low. However, when P_{sat} becomes high (e.g., 10^{-4}) or more than two constellations are employed, these fault modes must be monitored so as to ensure that the IR from unmonitored faults (P_{NM}) is smaller than P_{THRES}. In response, $\mathbb{L}_4^{\mathrm{V}}$ includes "dual SV faults from two constellations" hypotheses and "dual constellation faults" hypotheses. Consequently, the number of hypotheses in this list is extremely large, which mainly results from monitoring "dual SV faults" events.

Therefore, we present a fault grouping strategy for this list to reduce the number of monitored hypotheses. Fig. 8 shows the flowchart of the proposed strategy, and Table 9 summarizes the Grouping Units (GUs) that are used in this process. It is noteworthy that there are two choices for **GU3** for a dual-constellation combination, e.g., we can group "dual SV faults from GPS and BDS" to either "GPS constellation fault plus one BDS SV fault" or "BDS constellation fault plus one GPS SV fault". To elim-

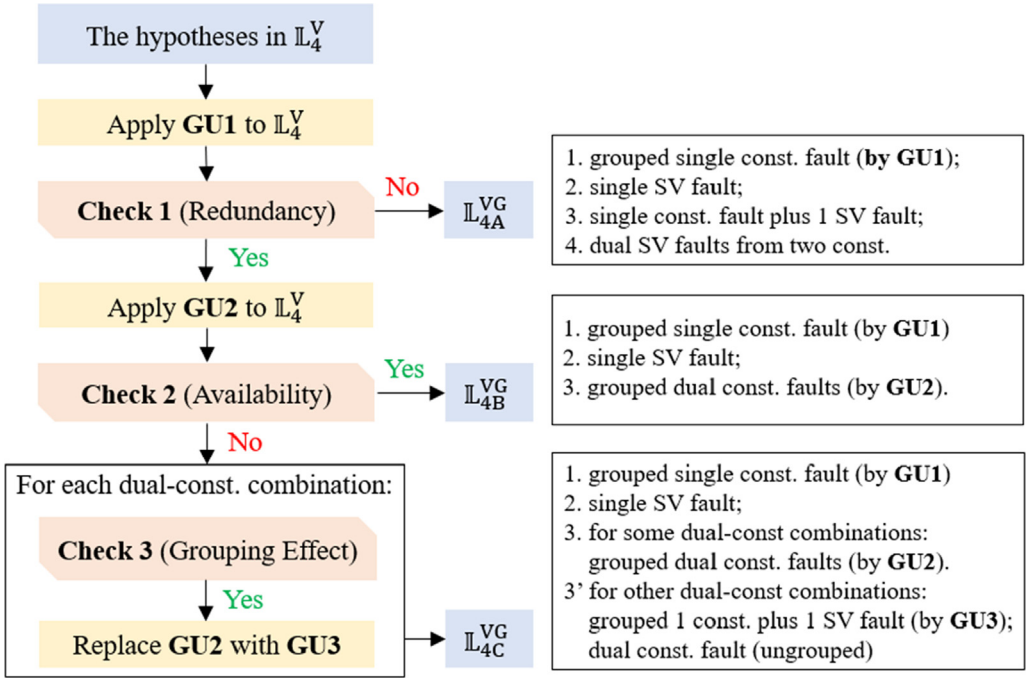

Fig. 8. Flowchart of the fault grouping strategy for List 4.

Table 9
Fault grouping units for List 4 in V-ARAIM.

Symbol	Description
GU1	Group "dual SV faults from one constellation" to "single constellation fault"
GU2	Group "dual SV faults from two constellations" and "one constellation fault plus one SV fault" into "dual constellation faults"
GU3	Group "dual SV faults from two constellations" into "one constellation fault plus one SV fault"

inate this ambiguity, we use the following criterion: if (a) constellation 1 has higher fault probability than constellation 2, or (b) their prior fault probabilities are similar while constellation 1 includes more visible SVs than constellation 2, then we group "dual SV faults from constellation 1 and constellation 2" to "constellation 1 fault plus one SV fault in constellation 2".

The proposed fault grouping strategy is illustrated as follows. First, for each constellation, we group "dual SV faults from one constellation" hypotheses to the constellation fault (i.e., **GU1**). Then, we perform **Check 1** to check whether there is enough redundancy to support monitoring dual constellation faults. If yes, go to the next step; otherwise, dual constellation faults need to be removed from the list and their probabilities should be added to P_{NM}. For the latter case, the fault modes that need to be monitored are given in $\mathbb{L}_{4A}^{VG}$, which is shown in Fig. 8.

If **Check 1** passes, then dual constellation faults are monitored, and we can implement **GU2** for each dual-constellation combination, i.e., grouping "dual SV faults from two constellations" and "single constellation fault plus one SV fault" to "dual constellation faults". Then we perform **Check 2** to check whether the final IR is below the target integrity risk, I_{REQ}. If this check passes, the final list of the monitored fault modes is given by $\mathbb{L}_{4B}^{VG}$, which includes the following hypotheses: (a) grouped single constellation fault (by **GU1**); (b) single SV fault; and (c) grouped dual constellation faults (by **GU2**).

If **Check 2** fails, we should perform **Check 3** as follows to determine whether it is possible to reduce the IR. For each dual-constellation combination, let us evaluate the impact of **GU2** on the IR. Using GPS-BDS as an example, we first check whether the following inequation holds:

$$IR_{k'}^{grp} - IR_{k}^{bsl} > P_{TOL} \tag{27}$$

where IR_{k}^{bsl} and $IR_{k'}^{grp}$ denote the IR contributions from the "GPS-BDS dual constellation faults" hypothesis before and after **GU2** is implemented, respectively. P_{TOL} is a tunable parameter, and it is preliminarily set to 5×10^{-9} in this work. If this inequation holds (i.e., **Check 3** passes), it means that applying **GU2** to GPS-BDS combination may seriously degrade the navigation performance. Therefore, for this dual-constellation combination, we replace **GU2** with **GU3** and leave the "GPS-BDS dual constellation faults" hypothesis monitored independently. As a reminder, **GU3** groups "dual SV faults from two constellations" into "single constellation fault plus one SV fault".

The final list, denoted by $\mathbb{L}_{4C}^{VG}$, is obtained after performing the above process for each dual-constellation combination. If (27) does not hold for any dual-constellation combination, it means that it is hard to improve the navigation performance for the current user geometry. In this case, we will output the IR associated with $\mathbb{L}_{4B}^{VG}$ to users, although this will lead to a LOC event.

As shown above, the proposed fault grouping strategy employs three checks to determine the final list of monitored fault modes. These checks are potentially beneficial to reducing the occurrence of the event that the implementation of fault grouping seriously degrades the navigation performance. It is also noteworthy that **Check 1** and **Check 2** hardly increase the computational burden, and Appendix proves that **Check 3** will neither bring much computational load to the system.

Table 10 shows the numbers of subsets after implementing fault grouping to V-ARAIM. Please note that the superscript "G" here indicates the list after fault grouping is applied. These numbers are evaluated at the same snapshot as that in Table 3. By comparing Table 3 with Table 10, we can find that the implementation of fault grouping can significantly reduce the computational load.

3.4. Modified fault grouping scheme for H-ARAIM FD

This subsection will provide an implementation of fault grouping to multi-constellation H-ARAIM. It has been widely agreed that negligible P_{const} of GPS can be applied for H-ARAIM whereas the wide faults of other constellations should be monitored (Walter et al. 2019). This is not an issue for the baseline MHSS, because the 8 MTs in Table 2 can cover all the H-ARAIM scenarios. But simply applying the V-ARAIM grouping scheme to H-ARAIM may result in $P_{NM} > P_{THRES}$ even after searching for all the lists given in Section 3.3. This is because the GPS constellation fault is not involved in H-ARAIM grouping, and thus "dual GPS SV faults" hypotheses directly contribute to P_{NM}. In response, the fault grouping scheme for V-ARAIM is modified as follows to support H-ARAIM.

For H-ARAIM, the lists of the monitored fault hypotheses before grouping and the corresponding fault grouping strategies for each list are illustrated as follows.

(1) $\mathbb{L}_1^H$: single SV fault; single non-GPS constellation fault

For each non-GPS constellation, we group "single SV fault" hypotheses into the constellation fault.

(2) $\mathbb{L}_2^H$: $\mathbb{L}_1^H$; dual SV faults from one non-GPS constellation

For each non-GPS constellation, we group "dual SV faults from one constellation" hypotheses into the constellation fault.

(3) $\mathbb{L}_3^H$: $\mathbb{L}_2^H$; single non-GPS constellation fault plus one SV fault from another constellation

We apply the same grouping operation as $\mathbb{L}_2^H$ to the hypotheses in this list.

(4) $\mathbb{L}_4^H$: $\mathbb{L}_3^H$; dual GPS SV faults

We apply the same grouping operation as $\mathbb{L}_2^H$ to the hypotheses in this list.

(5) $\mathbb{L}_5^H$: $\mathbb{L}_3^H$; dual SV faults from two constellations; dual non-GPS constellation faults

For this list, we follow the fault grouping strategy shown in Fig. 9, which is similar to that for V-ARAIM. The definitions of **GU1** $\sim$ **GU4** are given in Table 11, and the three checks are the same as those for V-ARAIM. Please note that the redundancy check (**Check 1**) always passes in H-ARAIM, because the GPS constellation fault is not monitored.

(6) $\mathbb{L}_6^H$: $\mathbb{L}_5^H$; dual SV faults from GPS

We apply the same grouping operation as $\mathbb{L}_5^H$ to the hypotheses in this list.

As a reminder, the user should first choose ONE of these lists through a search process, as shown in Fig. 7 (in Section 3.3), and then apply the associated fault grouping scheme shown above.

4. Exclusion candidates determination and grouping

The aim of an exclusion function is to reduce the continuity risk caused by true FD. The probability of a fault event occurring will increase when multiple constellations

Table 10
Numbers of monitored subsets of the proposed fault grouping scheme for V-ARAIM FD.

Constellations	Monitored List	Subset Number
GPS + GAL(N)	$\mathbb{L}_1^{VG}$	2
GPS + GAL(D)	$\mathbb{L}_{4A}^{VG}$	118
GPS + GAL(N) + BDS(N)	$\mathbb{L}_3^{VG}$	84
GPS + GAL(D) + BDS(D)	$\mathbb{L}_{4B}^{VG}$	33
GPS + GAL(N) + BDS(N) + GLO(N)	$\mathbb{L}_{4B}^{VG}$	44
GPS + GAL(N) + BDS(D) + GLO(D)	$\mathbb{L}_{4B}^{VG}$	44

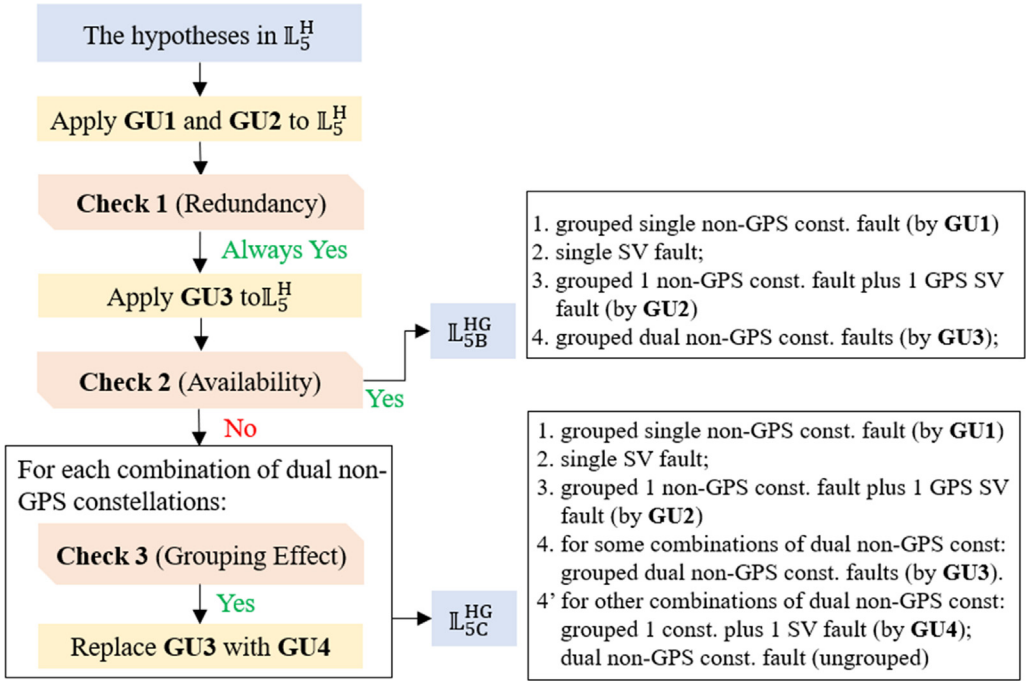

Fig. 9. Flowchart of the fault grouping strategy for List 5.

Table 11
Fault grouping units for List 5 in H-ARAIM.

Symbol	Description
GU1	Group "dual SV faults from one non-GPS constellation" into "single constellation fault";
GU2	Group "one GPS SV fault plus one SV fault from another constellation" into "one non-GPS constellation fault plus one GPS SV fault";
GU3	For each combination of two non-GPS constellations: group "dual SV faults from two constellations" and "one constellation fault plus one SV fault" into "dual constellation faults"
GU4	For each combination of two non-GPS constellations: group "dual SV faults from two constellations" into "one constellation fault plus one SV fault"

are employed, so more Exclusion Candidates (ECs) must be considered. This is similar to the determination of the monitored fault modes for integrity. Therefore, the grouping principle shown in Section 3 can also be applied to determine the ECs. In this section, the EC determination and grouping steps are established for H-ARAIM due to its operational need. However, these methodologies are also applicable for V-ARAIM exclusion.

Let P_{THRES}^{EC} be the threshold to determine whether a fault should be considered for exclusion, then:

$$P_{THRES}^{EC} = P_{alert} - P_{FANE,REQ} - P_{FDNE,REQ} \tag{28}$$

Accordingly, the exclusion function should ensure that a sufficient number of fault hypotheses are included in the EC sets, i.e.:

$$P_{NM}^{EC} < P_{THRES}^{EC}, \text{ where } P_{NM}^{EC} < 1 - P_{H,0}^{C} - \sum_{j=1}^{g_{bsl}} P_{H,j}^{C} \tag{29}$$

where g_{bsl} denotes the number of ECs in the baseline algorithm, and $P_{H,j}^{C}$ is the prior probability of the j th hypothesis in the EC set.

Continuity applies to average sense interpretation, and its requirement is less stringent than I_{REQ} (Joerger et al. 2020). Therefore, it can be verified that for multi-constellation ARAIM, the EC sets typically only include single SV exclusion, single constellation exclusion, and dual SV exclusion under the baseline MHSS architecture. Accordingly, Table 12 compares the EC sets before and after EC grouping is implemented.

For fault exclusion, we should (a) perform EC grouping and (b) implement fault grouping for the second layer hypotheses. Let us use an example to further illustrate this process. As an example for EC grouping, the ECs in $\mathbb{M}_j$ are grouped into the EC j to form a grouped EC j'. And for second layer hypothesis grouping, we assume that the second layer hypotheses in $\mathbb{M}_i$ are grouped into the hypothesis i to form a grouped hypothesis i'. Then, the prior probability of the grouped second layer hypothesis i' is updated in the same way as (20), as shown below:

$$P_{H,i'}^{grp} = P_{H,i} + \sum_{l \in \mathbb{M}_i} P_{H,l} \tag{30}$$

Table 12
Comparison of the EC sets in H-ARAIM FDE before and after EC grouping is implemented.

Set No.	Before Grouping (EC_{bsl})	After Grouping (EC_{grp})
1	Single SV exclusion, and single constellation exclusion	Single GPS SV exclusion, and single grouped non-GPS constellation exclusion
2	Exclusion of dual SVs	Exclusion of a single constellation plus a single SV from another constellation

where $P_{H,l}$ denotes the prior probability of H_l before grouping. At the same time, the FDNE budget for the i' th second layer detection event of EC j' is updated as follows:

$$P^{grp}_{FDNE,j',i'} = P_{FDNE,j,i} + \sum_{k\in\mathbb{M}_j}\sum_{l\in\mathbb{M}_i} P_{FDNE,k,l} \tag{31}$$

where $P_{FDNE,k,l}$ denotes the FDNE budget for the second layer detection event (k, l) before grouping, which is evaluated using (10). Accordingly, the test threshold for the second layer hypothesis (j', i'), i.e.,$T^{grp}_{j',i'}$, is updated using $P_{FDNE,j',i'}$ and (11). Please note that, (30) and (31) are also applicable to the case when the j th EC or the i th second layer hypothesis is not involved in the grouping process, as long as we set $\mathbb{M}_j$ or $\mathbb{M}_i$ to an empty set accordingly.

If we implement fault grouping to both FD and FE, the overall IR of FDE can be computed by:

$$IR^{grp}_{FDE} < IR^{grp}_{FD} + N^{ES}_{INT}\times \sum_{j=1}^{g_{grp}}\left(P\left(|\varepsilon_j| > \ell|H_0\right) + \sum_{\substack{i=1\\ s_i\subseteq s_j}}^{s_{grp}} P\left(|\varepsilon_j| > \ell|H_i\right)P^{grp}_{H,i} + \sum_{\substack{i=1\\ s_i\not\subset s_j}}^{s_{grp}} P\left(|\varepsilon_{j,i}| + T^{grp}_{j,i}\sigma_{\Delta_{j,i}} > \ell|H_i\right)P^{grp}_{H,i}\right) \tag{32}$$

where IR^{grp}_{FD} denotes the IR contribution of FD, which is evaluated using (22). Finally, Table 13 presents the numbers of subsets after applying the fault grouping schemes in Section 3 and Section 4 to ARAIM FDE. In this table, the superscript "G" indicates the list after fault grouping is applied. The results are obtained under the same settings as those in Table 3. By comparing Table 13 with Table 3, we can find that the implementation of fault grouping can effectively mitigate the computational issue.

5. Performance analyses

This section conducts multiple sets of simulations to evaluate the performance of the proposed implementation of fault grouping in different ARAIM operational scenarios. Section 5.1 shows the nominal simulation parameters, based on which Section 5.2 and Section 5.3 present the results for V-ARAIM FD and H-ARAIM FDE, respectively. Moreover, sensitivity analyses are carried out in Section 5.4, covering various constellation configurations and different ISM values. Note that being consistent with prior studies, the navigation performance is evaluated in terms of PLs and worldwide coverage.

5.1. Simulation Set-up

Table 14 describes the simulation conditions, and the numbers are modified from the commonly-used settings in prior studies (Blanch et al. 2015; EU-US Cooperation 2016). In addition to GPS and Galileo, BDS and GLONASS are involved for simulation. According to the latest official documents, the baseline BDS-3 constellation consists of 30 SVs whereas the baseline GLONASS constellation includes 24 SVs. The almanacs for BDS and GLONASS are made based on the information given by CelesTrak (i.e., https://celestrak.com/NORAD/elements/).

Table 15 lists the navigation requirements, nominal ISM values, and other simulation parameters. These values have been validated and justified in prior work (ICAO 2009; Walter et al. 2018; Walter et al. 2019; Joerger et al. 2020; Blanch et al. 2021). In Table 15, σ_{URA} is the standard deviation of the SISRE used for integrity, and b_{nom} denotes the nominal bias. All the simulation runs are carried out with MATLAB 2018b which is run on a desktop computer: CPU is i7-10700F and RAM is DDR4 16 GB.

5.2. Multi-Constellation V-ARAIM FD

This subsection analyzes the navigation performance of V-ARAIM FD. Nominal ISM values in Table 15 are

Table 13
Numbers of monitored subsets after applying the fault grouping technique to H-ARAIM FDE.

Constellations	Monitored List	EC Sets	Subset No.:$h_{grp}\times g_{grp}$
GPS + GAL(N)	$\mathbb{L}^{HG}_{3}$	1	243
GPS + GAL(D)	$\mathbb{L}^{HG}_{3}$	1	243
GPS + GAL(N) + BDS(N)	$\mathbb{L}^{HG}_{3}$	1	640
GPS + GAL(D) + BDS(D)	$\mathbb{L}^{HG}_{3}$	1, 2	2880
GPS + GAL(N) + BDS(N) + GLO(N)	$\mathbb{L}^{HG}_{5B}$	1	1276
GPS + GAL(N) + BDS(D) + GLO(D)	$\mathbb{L}^{HG}_{5B}$	1, 2	10,092

Table 14
Basic ARAIM simulation conditions.

Baseline Constellation	24 GPS + 24 GAL + 30 BDS + 24 GLO
Mask Angle	5°
User Grid	Latitude by Longitude: 10°×10°
Time Period	1 day
Time Steps	600 *sec*
MTTN	1 h
Error Model	Nominal models given by Blanch et al. (2015)
Coverage Range (Latitude)	V-ARAIM: −70° to 70°; H-ARAIM: −90° to 90°

applied for all the constellations, and the results are presented in terms of Vertical PL (VPL). Fig. 10 and Fig. 11 are the worldwide VPL maps respectively evaluated using the baseline MHSS and the fault grouping scheme. The results are summarized in the captions, which include constellation configurations, worldwide average VPL, 99.5 % availability coverage for LPV-200, and the average time consumption per epoch per user.

Both Fig. 10 and Fig. 11 show significant performance improvement by using more constellations. With four constellations, high coverage can be expected for a VAL as low as 15 m. More importantly, the comparison between these two figures suggests the comprehensive superiority of the fault grouping scheme over the baseline MHSS: in every case, the computational load is significantly lightened while the VPL values are also noticeably reduced.

5.3. Multi-Constellation H-ARAIM FDE

Similar to Section 5.2, this subsection presents the performance analysis results for H-ARAIM FDE. With nominal ISM values, the Horizontal PLs (HPLs) are evaluated using the baseline MHSS algorithm and the fault grouping scheme, and the worldwide HPL maps are respectively presented in Fig. 12 and Fig. 13. The general trend of these two figures is as expected, where the running time and average HPLs are simultaneously reduced using the fault grouping scheme. However, an in-depth comparison between Fig. 12a and Fig. 13a may lead to the question that why the former has fewer red regions whereas its general performance is worse, i.e., higher average HPL and lower availability coverage. To address this issue, the results are expressed in terms of availability in Fig. 14, and the reasons are given as follows.

Under the dual-constellation H-ARAIM scenario (Fig. 12a, 13a, and 14), the HPLs can easily go beyond 100 m. Therefore, Fig. 12a and Fig. 13a do not fully capture the actual performance difference – most areas are dark red. In addition, it is noteworthy that although the overall performance is improved by the fault grouping

Table 15
Navigation requirements and key simulation parameters for V- and H-ARAIM operations.

Parameters	V-ARAIM (LPV-200)	H-ARAIM (RNP 0.1)
I_{REQ}	10^{-7}/approach	10^{-7}/hour
P_{alert}	4×10^{-6}/15 *sec*	5×10^{-6}/hour
$P_{FA,REQ}/P_{FANE,REQ}$	3×10^{-6}/15 *sec*	2×10^{-6}/hour
$P_{FDNE,REQ}$	10^{-6}/15 *sec* (if needed)	2×10^{-6}/hour
Vertical AL (VAL)	35 *m*	N/A
Horizontal AL (HAL)	40 *m*	185 *m*
T_{EXP}	150 *sec*	1 h
N_{INT}^{ES}	1	360
N_{CON}^{ES}	1	360
P_{sat}	10^{-5}	10^{-5}
P_{const}	10^{-4}	GPS: 10^{-8} / Others:10^{-4}
σ_{URA}	1 *m*	2.4 *m*
b_{nom}	0.75 *m*	0.75 *m*

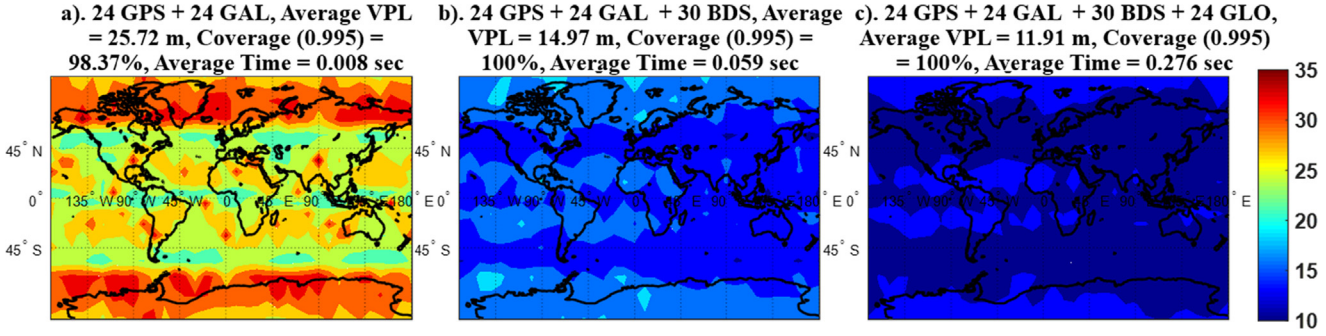

Fig. 10. VPL maps (in meters) of V-ARAIM FD using the baseline MHSS algorithm.

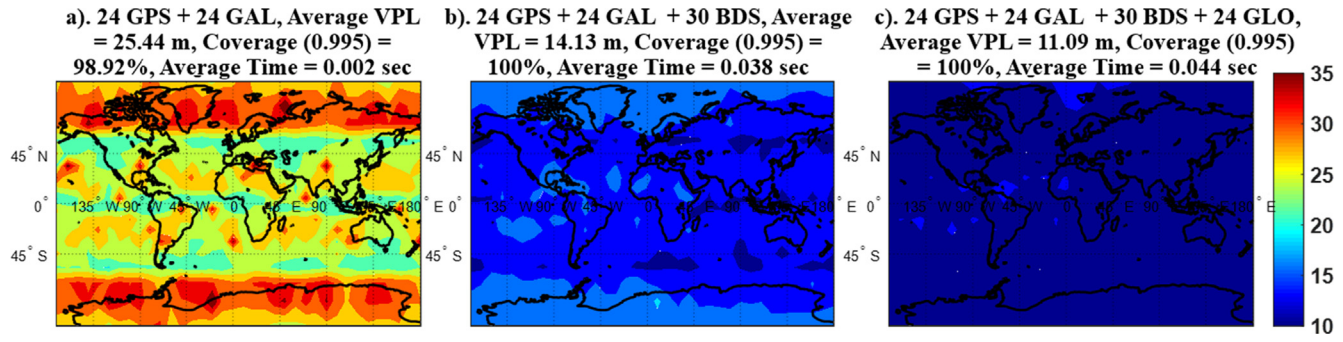

Fig. 11. VPL maps (in meters) of V-ARAIM FD using the fault grouping scheme.

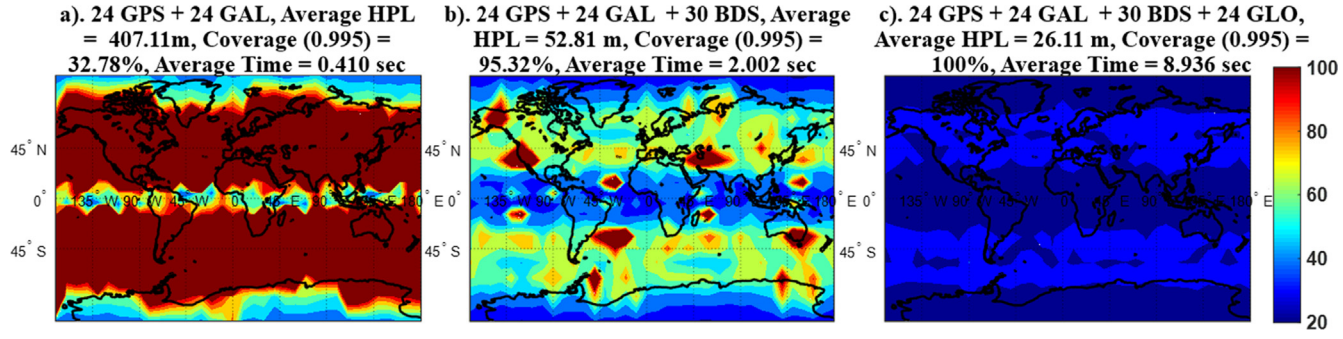

Fig. 12. HPL maps (in meters) of H-ARAIM FDE using the baseline MHSS scheme.

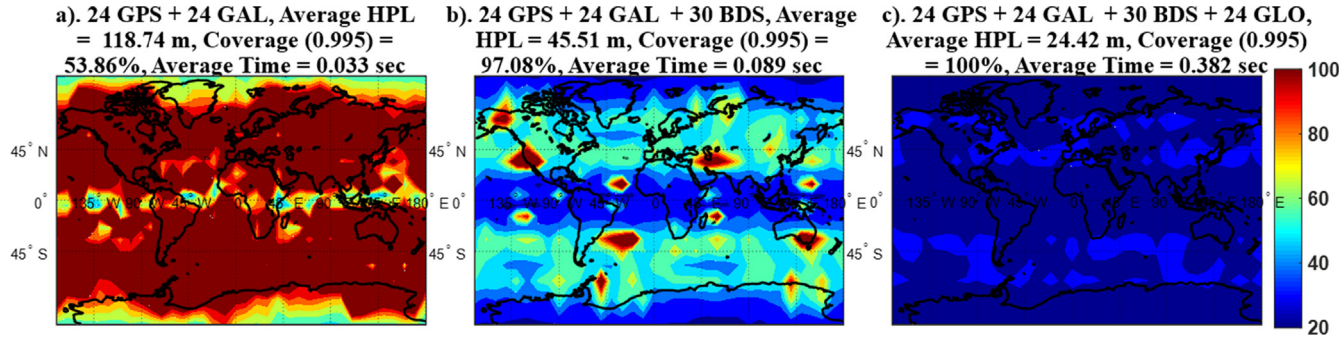

Fig. 13. HPL maps (in meters) of H-ARAIM FDE using the fault grouping scheme.

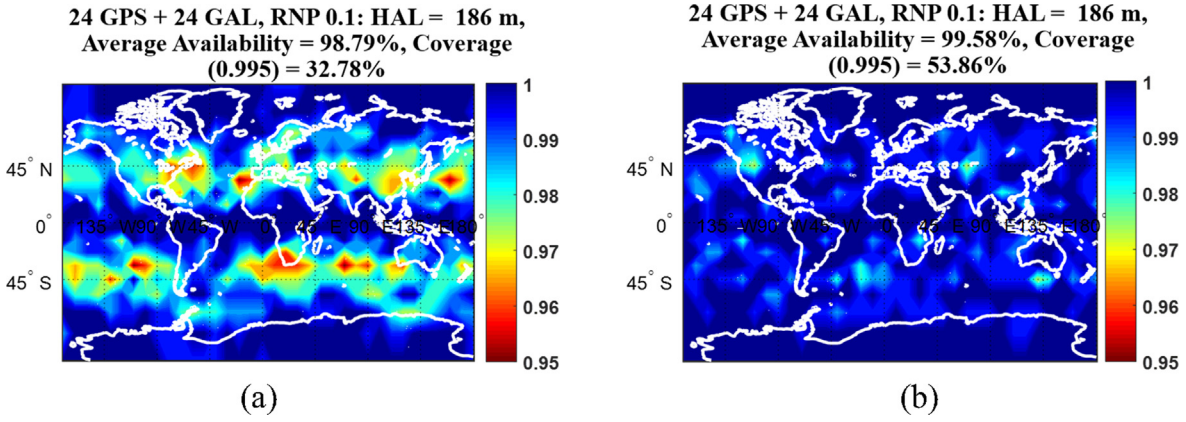

Fig. 14. Availability maps of dual-constellation H-ARAIM FDE using (a) the baseline MHSS scheme and (b) the fault grouping scheme.

Table 16
Overall navigation performance of V-ARAIM. For each set, the ISM is indicated by two rows: the top row gives the $-\log_{10}(P_{sat})$ / $-\log_{10}(P_{const})$ values, and the bottom row shows the σ_{URA} values.

Set	Constellations				FD/FDE	Average VPL (m)		Coverage (0.995)		Average Time (*sec*)	
	GPS	GAL	BDS	GLO		Baseline	Grouping	Baseline	Grouping	Baseline	Grouping
1	5/4	5/4	×	×	FD	25.72	25.44	98.37 %	98.92 %	0.0085	0.0024
	1.0	1.0	×	×							
2	5/4	4/4	×	×	FD	26.50	26.05	80.61 %	81.01 %	0.0226	0.0219
	1.0	1.0	×	×							
3	5/4	4/4	×	×	FD	40.34	40.01	2.31 %	2.61 %	0.0232	0.0223
	2.0	2.0	×	×							
4	5/4	5/4	5/4	×	FD	14.97	14.13	100 %	100 %	0.0592	0.0378
	1.0	1.0	1.0	×							
5	5/4	5/4	4/4	×	FD	19.23	18.59	100 %	100 %	0.0619	0.0224
	1.0	1.0	2.4	×							
6	5/4	4/4	4/4	×	FD	19.24	22.53	100 %	100 %	0.0620	0.0219
	1.0	1.0	2.4	×							
7	5/4	4/4	4/4	×	FD	22.29	23.12	100 %	100 %	0.0621	0.0220
	1.0	2.0	2.4	×							
8	5/4	5/4	4/4	×	FDE	38.26	35.88	37.17 %	44.68 %	2.5246	0.2752
	1.0	1.0	2.4	×							
9	5/4	4/4	4/4	×	FDE	38.32	37.41	37.17 %	39.09 %	2.5547	0.2757
	1.0	1.0	2.4	×							
10	5/4	5/4	5/4	5/4	FD	11.91	11.09	100 %	100 %	0.2761	0.0431
	1.0	1.0	1.0	1.0							
11	5/4	5/4	4/4	4/4	FD	16.75	15.46	100 %	100 %	0.2777	0.0451
	1.0	1.0	2.4	2.4							
12	5/4	4/4	4/4	4/4	FD	22.56	22.19	100 %	100 %	0.2904	0.0466
	1.0	2.0	2.4	10							
13	5/4	5/4	5/4	5/4	FDE	13.93	12.32	100 %	100 %	9.7569	0.1011
	1.0	1.0	1.0	1.0							
14	5/4	5/4	4/4	4/4	FDE	23.32	24.07	98.17 %	97.55 %	10.1212	0.1069
	1.0	1.0	2.4	2.4							

Table 17
Overall navigation performance of H-ARAIM FDE. For each set, the ISM is indicated by two rows: the top row gives the $-\log_{10}(P_{sat})$ / $-\log_{10}(P_{const})$ values, and the bottom row shows the σ_{URA} values.

Set	Constellations				FD/FDE	Average HPL (m)		Coverage (0.995)		Average Time (*sec*)	
	GPS	GAL	BDS	GLO		Baseline	Grouping	Baseline	Grouping	Baseline	Grouping
1	5/8	5/4	×	×	FDE	407.11	118.74	32.78 %	53.86 %	0.4096	0.0326
	2.4	2.4	×	×							
2	5/8	5/4	×	×	FDE	407.20	118.81	32.78 %	53.83 %	0.4111	0.0330
	2.4	6	×	×							
3	5/8	4/4	×	×	FDE	778.64	187.35	29.98 %	40.49 %	0.4247	0.0347
	2.4	2.4	×	×							
4	5/8	5/4	5/4	×	FDE	52.81	45.51	95.32 %	97.08 %	2.0021	0.0893
	2.4	2.4	2.4	×							
5	5/8	5/4	5/4	×	FDE	52.89	45.63	95.32 %	97.08 %	2.0041	0.0878
	2.4	6	4	×							
6	5/8	5/4	5/4	×	FDE	45.98	39.25	97.06 %	98.10 %	1.9920	0.0868
	2	6	4	×							
7	5/8	5/4	5/4	5/4	FDE	26.11	24.42	100 %	100 %	8.9365	0.3819
	2.4	2.4	2.4	2.4							
8	5/8	5/4	5/4	5/4	FDE	41.85	39.37	100 %	100 %	8.9410	0.3840
	2.4	6	4	18							
9	5/8	4/4	4/4	×	FDE	–	111.5	–	75.17 %	20.8333	0.3070
	2.4	2.4	2.4	×							
10	5/8	4/4	4/4	4/4	FDE	–	52.74	–	95.32 %	31.2500	2.4984
	2.4	2.4	2.4	2.4							

scheme, there exist snapshots where the fault grouping scheme leads to larger HPLs. The possible reasons are explained as follows. In the fault grouping scheme, we tend to avoid monitoring "dual GPS SV faults" and "dual SV faults from two constellations" hypotheses. This may significantly increase P_{NM}, or may force the user to monitor additional MTs (e.g., Galileo constellation fault plus a GPS SV fault) aside from those monitored in the baseline MHSS.

5.4. Sensitivity analysis of the overall navigation performance

In this subsection, sensitivity analyses are carried out to evaluate the performance of the proposed implementation of fault grouping under different ARAIM operational scenarios. Table 16 and Table 17 present the results for V-ARAIM and H-ARAIM, respectively, covering various constellation configurations and different ISM values. Note that the computational load is evaluated with the average computational time per epoch per user. Although this may slightly differ from the actual time consumption in airborne receivers, it is sufficient to reveal the effect of fault grouping on the reduction of computational burden.

Prior studies suggested that there are cases when FE is needed for V-ARAIM (Zhai et al. 2018; Joerger et al. 2020). Therefore, the anticipated performance of V-ARAIM FDE is also investigated for those three- or four-constellation scenarios with high prior probability. The results suggest that in most cases, the fault grouping scheme not only dramatically reduces the computational load but also improves the navigation performance. The reduction in computational load becomes more obvious when more constellations are employed, or FE is implemented. This is because, when more than two constellations are employed, grouping "dual SV faults from two constellations" and "single constellation fault plus one SV fault" into "dual constellation faults" can greatly reduce the number of subsets. Besides, for ARAIM FDE, fault grouping is applied to both the detection step and the exclusion step, and thus the reduction in computation load is more obvious than ARAIM FD. It is also noteworthy that there are several cases where the average VPLs slightly increase after applying the fault grouping scheme (i.e., sets 6, 7 and 14). This is because the reduction in the test thresholds cannot always compensate for the increase in the prior probabilities, especially when P_{sat} is large. Fortunately, these events are rare and their impact on navigation performance is negligible.

Similarly, the H-ARAIM results also suggest that the proposed implementation of fault grouping improves both efficiency and performance of ARAIM in most cases. Specifically, the computational load is significantly reduced by a factor of tens. Note that for the last two sets, the baseline algorithm needs to monitor the "dual SV faults" exclusion candidates, which makes the computational time become unrealistically long. Therefore, the corresponding results are not shown in Table 17.

6. Conclusions

This work presents and evaluates an implementation of fault grouping for MHSS ARAIM. Our contributions include two folds. First, we propose an implementation of fault grouping to ARAIM FDE, which can support up to four constellations. Specifically, the basic principles of fault grouping are revisited, and its impact on navigation performance is analyzed. Based on this, we implement the fault grouping technique to the fault detection step and the exclusion step in ARAIM, respectively, considering the difference between V-ARAIM and H-ARAIM scenarios.

The second contribution is evaluating the implementation of fault grouping with multiple sets of simulations. The simulations cover both V-ARAIM and H-ARAIM services and involve various constellation configurations and different ISM values. The results suggest that in most cases, the proposed implementation of fault grouping can effectively reduce the computational load while benefiting or maintaining the navigation performance. Therefore, the proposed approach is expected to accommodate most of the ARAIM operational scenarios. Future work includes (a) evaluating the proposed approach with more simulation scenarios and (b) incorporating other computational load reduction methods.

Declaration of Competing Interest

The authors declare that they have no known competing financial interests or personal relationships that could have appeared to influence the work reported in this paper.

Acknowledgments

The authors would like to thank Dr. Mathieu Joerger and Dr. Boris Pervan for their valuable suggestions and comments in the development of the algorithm. This work is supported by the Key Technologies Research and Development Program (2021YFB3901501) and the National Natural Science Foundation of China (62103274).

Appendix. Evaluation of the computational complexity of Check 3

This appendix provides a rough assessment on the computational complexity of **Check 3**. The implementation details of **Check 3** are given in Section 3.3. The computational load of this check mainly comes from (27). To evaluate its computation complexity, (27) is rewritten as follows:

$$\frac{IR_{k'}^{grp} - P_{TOL}}{N_{INT}^{ES} \cdot P_{H,k}} > P(|\varepsilon_k| + T_k\sigma_{\Delta_k} > \ell | H_k) \tag{A1}$$

Table A1
Average time consumption for calling Q^{-1}, Q, and least-squares estimation once.

Q^{-1} function	Q function	Least-squares estimation
1.1×10^{-6} *sec*	8.2×10^{-6} *sec*	5.8×10^{-6} *sec*

It further becomes:

$$Q^{-1}\left(\frac{IR_{k'}^{grp} - P_{TOL}}{N_{INT}^{ES} \cdot P_{H,k}}\right) < \frac{\ell - T_k \sigma_{\Delta_k} - b_k}{\sigma_k} \tag{A2}$$

with $T_k = Q^{-1}(P_{FA,k}/2)$.

Because $IR_{k'}^{grp}$ and σ_{Δ_k} have been computed while evaluating IR_{FD}^{grp}, they will not cause any additional computational cost. Therefore, the additional computational load mainly comes from calling the Q^{-1} function twice. Table A1 compares the time consumption of calling Q^{-1}, calling Q, and performing least-squares estimation in MATLAB. The least-squares estimation problem is established with 5 GPS SVs and 5 Galileo SVs (Blanch et al. 2015). The result proves that implementing **Check 3** will not bring much computational load, and it also explains why we use Q^{-1} instead of Q in (A2).

References

Bang, E., Milner, C., Macabiau, C., Estival, P. 2019. Sample temporal correlation effect on PHMI. In: Proceedings of the 2019 International Technical Meeting of The Institute of Navigation, Reston, VA, 85–99.

Blanch, J. et al., 2015. Baseline advanced RAIM user algorithm and possible improvements. IEEE Transactions on Aerospace and Electronic Systems 51 (1), 713–732.

Blanch, J., Walter, T., Enge, P. 2018. Fixed subset selection to reduce advanced RAIM complexity. In: Proceedings of the 2018 International Technical Meeting of The Institute of Navigation, Reston, VA, 88–98.

Blanch, J., Gunning, K., Walter, T., De Groot, L., Norman, L. 2019. Reducing computational load in solution separation for Kalman filters and an application to PPP integrity. In: Proceedings of the 2019 International Technical Meeting of The Institute of Navigation, Reston, VA, 720–729.

Blanch, J., Liu, X., Gunning, K., and Walter, T. 2021. Analysis of GNSS constellation performance for advanced RAIM. In: Proceedings of the 34th International Technical Meeting of The Satellite Division of the Institute of Navigation (ION GNSS+ 2021), St. Louis, MO, 1410–1434.

Blanch, J., Walter, T., Enge, P., 2017. Protection levels after fault exclusion for advanced RAIM. Navigation 64 (4), 505–513.

Blanch, J., Walter, T., 2021. Fast protection levels for fault detection with an application to advanced RAIM. IEEE Transactions on Aerospace and Electronic Systems 57 (1), 55–65.

Blanch, J., et al. 2014. Architectures for advanced RAIM: offline and online. Proceedings of the 27th International Technical Meeting of The Satellite Division of the Institute of Navigation (ION GNSS+ 2014), Tampa, FL, 787–804.

Blanch, J, et al. 2022. Baseline advanced RAIM user algorithm: proposed updates. Proceedings of the 2022 International Technical Meeting of The Institute of Navigation, Long Beach, CA, 229–251.

Brown, R.G., 1992. A baseline GPS RAIM scheme and a note on the equivalence of three RAIM methods. Navigation 39 (3), 301–316.

Cassel, R., 2017. Real-time ARAIM using GPS, GLONASS and GALILEO. Illinois Institute of Technology, M.S. Dissertation,.

El-Mowafy, A., 2016. Pilot evaluation of integrating GLONASS, Galileo and BeiDou with GPS in ARAIM. Artificial Satellites 51 (1), 31–44.

El-Mowafy, A., Yang, C., 2016. Limited sensitivity analysis of ARAIM availability for LPV-200 over Australia using real data. Advances in Space Research 57 (2), 659–670.

EU-US Cooperation, 2016. ARAIM technical subgroup milestone 3 report. E.U.-U.S. Cooperation on Satellite Navigation, Working Group C. Available at: http://www.gps.gov/policy/cooperation/europe/2016/working-group-c/ARAIM-milestone-3-report.pdf.

Ge, Y., Wang, Z., Zhu, Y., 2017. Reduced ARAIM monitoring subset method based on satellites in different orbital planes. GPS Solutions 21 (4), 1443–1456.

GPS World, 2014. The system: GLONASS in April, what went wrong. GPS World, June 24, 2014. Available at: https://www.gpsworld.com/the-system-glonass-in-april-what-went-wrong/.

Gunning, K., Blanch, J., Walter, T., de Groot, L., Norman, L. 2019. Integrity for tightly coupled PPP and IMU. In: Proceedings of the 32nd International Technical Meeting of the Satellite Division of The Institute of Navigation (ION GNSS+ 2019), Miami, FL, 3066–3078.

International Civil Aviation Organization (ICAO), 2009. Annex 10, Aeronautical telecommunications, volume 1 (radio navigation aids), amendment 84, Montreal, QC, Canada.

Inside GNSS, 2019. Lessons to be learned from Galileo signal outage. Inside GNSS, October 1, 2019. Available at: https://insidegnss.-com/lessons-to-be-learned-from-galileo-signal-outage/.

Joerger, M., Chan, F.-C., Pervan, B., 2014. Solution separation versus residual-based RAIM. Navigation 61 (4), 273–291.

Joerger, M., Zhai, Y., Martini, I., Blanch, J., Pervan, B. 2020. ARAIM continuity and availability assertions, assumptions, and evaluation methods. In: Proceedings of the 2020 International Technical Meeting of The Institute of Navigation, San Diego, CA, 404–420.

Joerger, M., Pervan, B., 2016. Fault detection and exclusion using solution separation and chi-squared RAIM. IEEE Transactions on Aerospace and Electronic Systems 52 (2), 726–742.

Khanafseh, S., Joerger, M., Chan, F.-C., Pervan, B., 2015. ARAIM integrity support message parameter validation by online ground monitor. The Journal of Navigation 68 (2), 327–337.

Lee, Y., Braff, R., Fernow, J. P., Hashemi, D., McLaughlin, M., O'Laughlin, D. 2005. GPS and Galileo with RAIM or WAAS for vertically guided approaches. In: Proceedings of the 18th International Technical Meeting of the Satellite Division of The Institute of Navigation (ION GNSS 2005), Long Beach, CA, 1801–1825.

Lee, Y. 2006. A New Improved RAIM Method Based on the Optimally Weighted Average Solution (OWAS) Under the Assumption of a Single Fault. In: Proceedings of the 2006 National Technical Meeting of The Institute of Navigation, Monterey, CA, 574–586.

Luo, S. et al., 2020. Satellite selection methods for multi-constellation advanced RAIM. Advances in Space Research 65 (5), 1503–1517.

Meng, Q., Liu, J., Zeng, Q., Feng, S., Xu, R., 2019. Improved ARAIM fault modes determination scheme based on feedback structure with probability accumulation. GPS Solutions 23, 16.

Milner, C., Bang, E., Macabiau, C., Estival, P. 2017. Methods of integrity risk computation for ARAIM FDE. In: Proceedings of the 30th International Technical Meeting of The Satellite Division of the Institute of Navigation, Portland, OR, 2371–2387.

Milner, C., Pervan, B., Blanch, J., Joerger, M. 2020. Evaluating integrity and continuity over time in advanced RAIM. 2020 IEEE/ION Position, Location and Navigation Symposium (PLANS), Portland, OR, 502–514.

Orejas, M., Skalicky, J., Ziegler, U. 2016. Implementation and testing of clustered ARAIM in a GPS/Galileo receiver. In: Proceedings of the 29th International Technical Meeting of the Satellite Division of The Institute of Navigation (ION GNSS+ 2016), Portland, OR, 1360–1367.

Orejas, M., Skalicky, J., 2016. Clustered ARAIM. Proceedings of the 2016 International Technical Meeting of the Institute of Navigation.

Pan, W., Zhan, X., Zhang, X., Wang, S., 2019. A subset-reduced method for FDE ARAIM of tightly-coupled GNSS/INS. Sensors 19 (22), 4847.

Perea, S., Meurer, M., Rippl, M., Belabbas, B., Joerger, M., 2017. URA/SISA Analysis for GPS and Galileo to support ARAIM. Navigation 64 (2), 237–254.

Pervan, B., 1996. Navigation integrity for aircraft precision landing using the global positioning system. Stanford University, Ph.D. Dissertation.

Walter, T., Blanch, J., Enge, P. 2014. Reduced subset analysis for multi-constellation ARAIM. In: Proceedings of the 2014 International Technical Meeting of The Institute of Navigation, San Diego, CA, 89–98.

Walter, T., Gunning, K., Phelts, E., Blanch, J., 2018. Validation of the unfaulted error bounds for ARAIM. Navigation 65 (1), 117–133.

Walter, T., Blanch, J., Gunning, K., Joerger, M., Pervan, B., 2019. Determination of fault probabilities for ARAIM. IEEE Transactions on Aerospace and Electronic Systems 55 (6), 3505–3516.

Wang, E. et al., 2018. Fault detection and isolation in GPS receiver autonomous integrity monitoring based on chaos particle swarm optimization-particle filter algorithm. Advances in Space Research 61 (5), 1260–1272.

Wang, S., Zhai, Y., Zhan, X., 2021. Characterizing BDS signal-in-space performance from integrity perspective. Navigation 68 (1), 157–183.

Yang, Y. et al., 2022. Principle and performance of BDSBAS and PPP-B2b of BDS-3. Satellite Navigation 3 (5), 1–9.

Zhai, Y., Joerger, M., Pervan, B., 2018. Fault exclusion in multi-constellation global navigation satellite systems. The Journal of Navigation 71 (6), 1281–1298.

Zhai, Y., Zhan, X., Chang, J., Pervan, B., 2019a. ARAIM with more than two constellations. Proceedings of the ION 2019 Pacific PNT Meeting.

Zhai, Y., Zhan, X., Pervan, B., 2019b. Bounding integrity risk and false alert probability over exposure time intervals. IEEE Transactions on Aerospace and Electronic Systems 56 (3), 1873–1885.

Zhai, Y., Patel, J., Zhan, X., Joerger, M., Pervan, B., 2020. An Advanced Receiver Autonomous Integrity Monitoring (ARAIM) ground monitor design to estimate satellite orbits and clocks. The Journal of Navigation 73 (5), 1087–1105.